machines

MDPI

Article

Unified Kinematic and Rigid-Body Dynamic Modeling of an XYZAC Five-Axis Machine Tool via Task-to-Screw-Space Mapping

Ye Wei *, Taiyong Wang, Jing Kang and Ying Tian

School of Mechanical Engineering, Tianjin University, Tianjin 300354, China
* Correspondence: yewei0116@tju.edu.cn

Abstract

Aunified analytical framework is developed for an XYZAC five-axis CNC machine tool to establish a physically consistent connection between practical machining-task variables, rigid-body screw motion, and inverse dynamics. The tool-tip/tool-axis task is represented in $\mathbb{R}^3 \times S^2$, while the product-of-exponentials formulation is used to establish the forward- and inverse-position kinematics. A topology-constrained two-stage mapping converts the machining-task rate first into the actual six-dimensional rigid-body twist and subsequently into the five generalized axis velocities. A supplementary constrained motion screw and reciprocal screw/wrench duality are employed to construct the corresponding analytical inverse. At the acceleration level, task-space geometric effects and mechanism-configuration effects are explicitly separated, after which the generalized states are coupled with the physical rigid-body chains through Newton–Euler equations and virtual work. A singularity analysis gives $\sigma_{\min} = |\sin q_A|$ and $\kappa_2 = 1/|\sin q_A|$, quantitatively revealing the degeneration of the orientation mapping as $q_A \to 0$. Closed-loop kinematic validation yields maximum RMSEs of 3.811000×10^{-14} mm and 2.657723×10^{-15} deg and maximum absolute errors below 1.110223×10^{-13} mm and 1.272222×10^{-14} deg, while force/torque benchmarking gives maximum RMSEs of 0.0821185 N and 1.39897 N·mm and maximum absolute errors of 0.531176 N and 8.76912 N·mm relative to simulation. The results demonstrate consistent task-to-motion-to-load propagation within the investigated rigid-body regime and provide a unified interface for subsequent elastodynamic and machining-load coupling analyses.

Keywords: five-axisCNC machine tool; screw theory; product of exponentials (POE); differential kinematics; rigid-body dynamics; Newton–Euler formulation

Check for updates

Academic Editor: Zhuming Bi

Received: 20 September 2026
Revised: 14 October 2026
Accepted: 19 October 2026
Published: 22 October 2026

Copyright: © 2026 by the authors. Licensee MDPI, Basel, Switzerland. This article is an open access article distributed under the terms and conditions of the Creative Commons Attribution (CC BY) license.

1. Introduction

Five-axis CNC machining enables the simultaneous control of the tool-tip position and tool-axis orientation during complex surface manufacturing through the coordinated motion of three translational axes and two rotary axes. It has been widely employed in the high-precision fabrication of complex components, including blades, impellers, molds, and other free-form surfaces [1–3]. Unlike three-axis machining, five-axis CAM tool-path data generally contain both the tool-tip position and the unit tool-axis direction. Therefore, the CNC controller must transform the machining task defined in the workpiece coordinate frame into motion commands of the translational and rotary axes through kinematic transformations [4–6]. From a geometric perspective, the tool-tip position belongs to the Euclidean space $\mathbb{R}^3$, whereas the unit tool-axis direction lies on the unit sphere S^2. Together, these two components constitute

a machining-task representation with five independent degrees of freedom [7]. Huang et al. planned the translational and angular motions in five-axis machining separately within $\mathbb{R}^3$ and S^2, respectively, further demonstrating that tool-tip translation and tool-axis orientation variation possess distinct geometric characteristics [6].

For the kinematic analysis of five-axis machine tools, systematic theoretical foundations have been established through extensive research. Sørby derived analytical forward- and inverse-kinematic models for five-axis machine tools with non-orthogonal rotary axes and investigated the axis motion behavior near singular configurations [5]. Yang and Altintas employed screw theory to develop a generalized kinematic formulation applicable to various serial five-axis machine tool architectures. By using the product-of-exponentials (POE) formulation, translational and rotational joints were uniformly represented, providing an important foundation for the configuration-independent kinematic modeling of five-axis machine tools [4]. Subsequently, My and Bohez developed a general five-axis CNC kinematic model from the perspective of differential kinematics and evaluated the motion performance of different machine configurations based on Jacobian properties [8]. Recently, Lu et al. further demonstrated that, for AC-type five-axis machine tools, representing tool-axis orientation on S^2 and describing complete rigid-body orientation through $SO(3)$ exhibit different characteristics in terms of singularity behavior and rotary-axis motion smoothness. They further investigated the tool-axis-direction Jacobian and the actual angular-velocity Jacobian, respectively [9]. These studies have established a solid foundation for the position- and velocity-level kinematic analysis of five-axis machine tools. However, they also reveal a critical issue: the time derivative of the tool-axis direction is not equivalent to the actual spatial angular velocity of the rigid body.

From the perspective of rigid-body motion theory, the POE formulation not only describes finite rigid-body configurations but also continuously generates instantaneous motion screws through the differential relationship between the Lie group $SE(3)$ and its associated Lie algebra $\mathfrak{se}(3)$ [10]. Müller systematically investigated the higher-order kinematic relationships of POE-based lower-pair motion chains and demonstrated that the higher-order derivatives of spatial Jacobian columns with respect to joint variables and time can be uniformly represented using Lie brackets and adjoint operators [11]. For five-degree-of-freedom $3T2R$ mechanisms, since the admissible motion space constitutes only a five-dimensional subspace of the six-dimensional instantaneous rigid-body motion space, reciprocal screw/wrench theory has been employed to extract the actuated motion subspace, constrained motion subspace, and singularity characteristics [12]. These studies provide the established mathematical foundations for finite, first-order, and higher-order rigid-body motion descriptions in screw coordinates. In the present study, these relations are employed as theoretical building blocks for constructing the machine-specific mapping interfaces described below [13,14].

On the other hand, screw theory possesses an inherent power–duality relationship between motion and force and has been widely applied to the dynamic modeling of rigid bodies and multibody systems. Selig introduced screw coordinates for describing the dynamics of rigid bodies and serial robotic systems [15], while Gallardo et al. further combined screw theory with the principle of virtual work to formulate the driving forces of mechanisms [16]. For five-axis machine tools, Huynh and Altintas developed a multibody dynamic model incorporating the major moving components, mass properties, inertia parameters, and structural flexibility of the machine tool, enabling the characterization of pose-dependent dynamic behaviors [17]. Subsequently, they integrated tool-path generation, inverse kinematics, drive control, and multibody structural dynamics of five-axis machine tools to predict motion and vibration responses under practical machining trajectories [18]. Bilgili et al. improved the computational efficiency of pose-dependent multibody dynamic analysis for five-axis machine tools through Jacobian-based substructure assembly techniques [19]. These studies

primarily address pose-dependent structural dynamics, controller–structure interaction, and computational efficiency, respectively, with the dynamic models generally formulated from joint states, control variables, or structural coordinates. The explicit transformation from practical tool-tip/tool-axis task variables to the rigid-body motion quantities required by these dynamic formulations is not their primary focus [20,21]. To further clarify the relationships between the existing studies and the present work, a comparative summary of their main contributions, research scope, and limitations is provided in Table 1.

Table 1. Comparison of representative studies with the present work.

Reference	Main Focus	Established Contribution	What Is Not the Primary Focus of That Work	Role Relative to the Present Study
Yang and Altintas [4]	General five-axis screw kinematics	Generalized screw-based forward/inverse kinematics; C^3 tool path and singularity avoidance	Explicit task-rate $\rightarrow$ actual twist $\rightarrow$ rigid-body dynamics interface	Established kinematic foundation
My and Bohez [8]	Differential kinematics	Generalized differential model and kinematic-performance indices for five-axis configurations	Rigid-body dynamic interface and task-space second-order decomposition	Established differential-kinematic foundation
Lu et al. [9]	Orientation smoothing/singularity	SO(3)-based smoothing, singularity sensitivity, and rotary-axis velocity/acceleration/jerk improvement	Task-to-rigid-body inverse-dynamics integration	Related orientation/singularity study
Müller [11]	Higher-order screw kinematics	General higher-order POE relations using Lie brackets and adjoint operators	Five-axis-specific $\mathbb{R}^3 \times S^2$ machining-task interface	Established mathematical foundation
Huynh and Altintas [17]	Multibody dynamics	Pose-dependent flexible multibody machine-tool model with structural flexibility	Explicit $\mathbb{R}^3 \times S^2 \rightarrow \mathfrak{se}(3)$ task mapping	Established multibody-dynamic framework
Huynh and Altintas [18]	Controller–structure dynamics	Tool path, inverse kinematics, servo control, and flexible structural dynamics integrated for vibration prediction	Analytical separation of task-space and topology-induced second-order terms	Established integrated dynamic framework
Bilgili et al. [19]	Efficient multibody dynamics	Reduced-order substructure assembly and computationally efficient pose-dependent dynamics	Practical task-to-screw interface	Established efficient dynamic framework
Present study	Interface consistency	$\mathbb{R}^3 \times S^2 \rightarrow \mathfrak{se}(3) \rightarrow \mathbf{q} \rightarrow$ physical rigid-body chains; first-/second-order mapping; rigid-body inverse forces/torques	Structural flexibility and servo dynamics are outside the current scope	New integration architecture and mapping interfaces

Accordingly, the research gap addressed in this study does not lie in the absence of screw-based generalized kinematics, higher-order POE relations, reciprocal screw/wrench theory, or multibody dynamic formulations themselves, since these theoretical foundations have already been well established in the literature. Rather, the unresolved issue considered here is the interface consistency among four different modeling levels: (i) the practical tool-tip/tool-axis machining task represented in $\mathbb{R}^3 \times S^2$; (ii) the six-dimensional rigid-body motion screw required by screw-based differential kinematics and dynamics; (iii) the five-dimensional generalized joint-motion space of the actuated XYZAC axes; and (iv) the physical rigid-body chains required by inverse dynamics. In particular, the tool-axis-direction rate is not itself a spatial angular velocity, while a direct task-Jacobian formulation generally combines the second-order geometric contribution associated with task parameterization with the configuration-dependent contribution associated with the mechanism Jacobian. The present study therefore focuses on constructing explicit and physically consistent interfaces among these modeling levels.

To this end, an XYZAC five-axis CNC machine tool is selected as the research object in this study. First, the machining task variables are defined by the tool-tip position and tool-axis unit direction, and analytical forward- and inverse-position solutions are established based on the POE finite motions of the tool-side XYZ kinematic chain and workpiece-side AC kinematic chain. Subsequently, the differential relationship of the tool-axis direction is coupled with the admissible angular motion subspace spanned by the two AC rotary axes of the current mechanism, leading to a constraint-aware mapping from first-order machining task variables to the actual six-dimensional motion screw. For the 6×5 non-square mapping formed by the five admissible motion screws, an additional constrained motion screw is introduced to construct a complete six-dimensional motion screw basis, and an analytical left inverse is obtained through the reciprocal wrench–screw duality. Furthermore, by separately differentiating the task-variable-to-screw mapping and the POE-based admissible motion screw mapping, the second-order terms $\dot{\mathbf{L}}_v\dot{\mathbf{x}}$ and $\dot{\mathbf{T}}\dot{\mathbf{q}}$ are explicitly interpreted as the second-order contributions induced by the variation of machining task geometry and mechanism configuration, respectively. Consequently, a differential kinematic model with consistent position–velocity–acceleration transmission is established. Finally, the actual physical POE chains of individual moving bodies with respect to the fixed machine bed are recovered, and a rigid-body inverse dynamics model for the five-axis machine tool is formulated using the Newton–Euler equations and the power duality between motion screws and force screws.

The main contributions of this study can be summarized as follows. The contributions of this study lie in the construction and integration of the mapping interfaces connecting the machining-task representation, rigid-body screw motion, generalized axis states, and physical rigid-body dynamics. First, a topology-constrained task-to-screw mapping is constructed between the practical tool-tip/tool-axis machining task represented in $\mathbb{R}^3 \times S^2$ and the six-dimensional rigid-body motion-screw space. Rather than directly identifying the tool-axis-direction rate with a spatial angular velocity, the proposed mapping reconstructs the physically admissible relative angular velocity through the instantaneous allowable rotational subspace of the A and C axes. This establishes a physically consistent interface from the machining-task variables to the rigid-body motion representation required by subsequent screw-based kinematics and dynamics. Second, topology-dependent two-stage analytical mapping is established from the machining-task rate to the five actuated generalized velocities, $\dot{\mathbf{x}}_t^{(w)} \rightarrow \boldsymbol{\nu}_t^{(w)} \rightarrow \dot{\mathbf{q}}$. The first stage converts the practical machining-task variables into an actual six-dimensional rigid-body motion screw, whereas the second stage maps this screw to the five-dimensional actuated motion through the allowable-motion screw basis of the XYZAC topology. To resolve the non-square 6×5 mapping, a supplementary constrained motion screw is introduced to complete the six-dimensional screw basis, after which the established reciprocal screw/wrench duality is employed to construct the corresponding analytical left inverse. The contribution therefore lies in the topology-specific construction and integration of the two mapping stages rather than in reciprocal screw/wrench theory itself. At the second-order motion level, the geometric contribution induced by the time variation of the task-to-screw mapping and the mechanism contribution induced by the configuration-dependent variation of the allowable-motion screw basis are explicitly separated as $\dot{\mathbf{L}}_{v,t}^{(w)}\dot{\mathbf{x}}_t^{(w)}$ and $\dot{\mathbf{T}}_t^{(w)}\dot{\mathbf{q}}$, respectively. The resulting generalized position, velocity, and acceleration states are then transferred from the relative tool–workpiece task chain to the actual physical kinematic chains of the moving machine components and coupled with the classical Newton–Euler and virtual-work formulations. This provides a continuous analytical interface from machining-task motion to the generalized driving forces and torques while keeping task-space geometric effects and mechanism-configuration effects physically distinguishable.

2. Mechanism Description

A unified screw-based kinematic and rigid-body dynamic model is established in this study for an XYZAC five-axis CNC machine tool. Starting from the special Euclidean group $SE(3)$, the Lie algebra $\mathfrak{se}(3)$, motion screws, wrench screws, and their adjoint/dual transformations, the five actuated axes of the XYZAC machine tool are uniformly treated as five one-DOF screw-motion units.

The tool-side kinematic chain of the target machine tool is given by

$$B_0 \rightarrow B_Y \rightarrow B_X \rightarrow B_Z \rightarrow B_t \tag{1}$$

The workpiece-side kinematic chain is given by

$$B_0 \rightarrow B_A \rightarrow B_C \rightarrow B_w \tag{2}$$

The five independent motion DOFs of the machine tool are uniformly defined as

$$\mathbf{q} = \begin{pmatrix} q_X & q_Y & q_Z & q_A & q_C \end{pmatrix}^T \tag{3}$$

Figure 1 shows the CAD model and schematic representation of the five-axis CNC machine tool. The motions of the machine components can be described with respect to the machine-bed coordinate frame. The left–right motion of the spindle is defined as the X-axis motion, with the leftward direction taken as positive; the forward–backward motion is defined as the Y-axis motion, with the forward direction taken as positive; and the vertical motion is defined as the Z-axis motion, with the upward direction taken as positive.

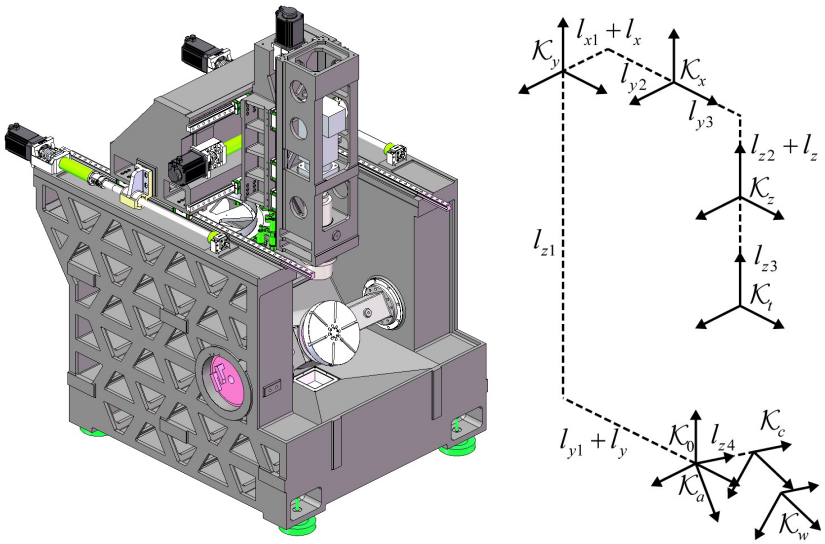

(**a**) (**b**)

Figure 1. Five-axis CNC machine tool: (**a**) CAD model. (**b**) Dschematic diagram of the mechanism.

The machine bed is fixed to the ground, and the machine-bed coordinate frame $O_0 - x_0y_0z_0$ is denoted by $\mathcal{K}_0$. Its origin O_0 is located at the intersection between the rotary-table axis and the central axis of the worktable. The x_0, y_0, and z_0 axes are aligned with the X-, Y-, and Z-axis directions of the machine tool, respectively.

The coordinate frame $O_y - x_yy_yz_y$ attached to the Y-axis moving module is denoted by $\mathcal{K}_y$ Its origin O_y is located at the intersection between the centerline of the ball-screw shaft driving the X axis and the y_0z_0 plane. The x_y, y_y, and z_y axes are aligned with the X-, Y-, and Z-axis directions, respectively. In $\mathcal{K}_0$, point O_1 is located at a distance of $l_{y1} + l_y$

from O_0 along the negative y_0 direction, while O_y is located at a distance of l_{z1} from O_1 along the positive z_0 direction.

The coordinate frame $O_x - x_x y_x z_x$ attached to the X-axis moving module is denoted by $\mathcal{K}_x$. Its origin O_x is located at the intersection between the centerline of the ball-screw shaft driving the Z-axis and the $x_y y_y$ plane. The x_x, y_x, and z_x axes are aligned with the X-, Y-, and Z-axis directions, respectively. In $\mathcal{K}_y$, point O_2 is located at a distance of $l_{x1} + l_x$ from O_y along the negative x_y direction, while O_x is located at a distance of l_{y2} from O_2 along the positive y_y direction.

The coordinate frame $O_z - x_z y_z z_z$ attached to the Z-axis moving module and spindle is denoted by $\mathcal{K}_z$. Its origin O_z is located at the intersection between the mid-height plane of the Z-axis moving module and the $y_x z_x$ plane. The x_z, y_z, and z_z axes are aligned with the X-, Y-, and Z-axis directions, respectively. In $\mathcal{K}_x$, point O_3 is located at a distance of l_{y3} from O_x along the positive y_x direction, whereas O_z is located at a distance of $l_{z2} + l_z$ from O_3 along the negative z_x direction.

The tool coordinate frame $O_t - x_t y_t z_t$ is denoted by $\mathcal{K}_t$, with its origin located at the tool tip. The x_t, y_t, and z_t axes are aligned with the X-, Y-, and Z-axis directions, respectively. In $\mathcal{K}_z$, point O_t is located at a distance of l_{z3} from O_z along the negative z_z direction.

The rotary-table coordinate frame $O_a - x_a y_a z_a$ is denoted by $\mathcal{K}_a$. Its origin O_a coincides with O_0, and the x_a axis coincides with the x_0 axis. The y_a and z_a axes are obtained by rotating the y_0 and z_0 axes, respectively, about the x_0 axis through α.

The worktable coordinate frame $O_c - x_c y_c z_c$ is denoted by $\mathcal{K}_c$. Its origin, O_c, is located at a distance of l_{z4} from O_a along the positive z_a direction in $\mathcal{K}_a$. The z_c axis coincides with the z_a axis, whereas the x_c and y_c axes are obtained by rotating the x_a and y_a axes, respectively, about the z_a axis through γ.

The workpiece coordinate frame $O_w - x_w y_w z_w$ is denoted by $\mathcal{K}_w$. The coordinates of its origin O_w expressed in $\mathcal{K}_c$ are $\begin{pmatrix} x_{w0} & y_{w0} & z_{w0} \end{pmatrix}^T$. The x_w, y_w, and z_w axes are aligned with the x_c, y_c, and z_c axes, respectively.

The coordinate frames of the machine-tool components and their corresponding rotation matrices are summarized in Table 2.

Table 2. Coordinate frames of the components in the kinematic chains.

	Coordinate Frame	Rotation Matrix
Machine bed	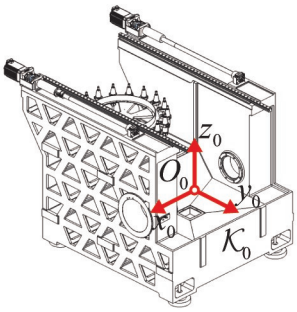	$\mathbf{R}_0$
Y-axis moving module	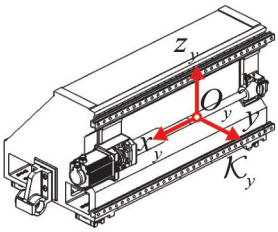	$\mathbf{R}_y = \mathbf{R}_0$

Table 2. *Cont.*

	Coordinate Frame	Rotation Matrix
X-axis moving module Z-axis moving module	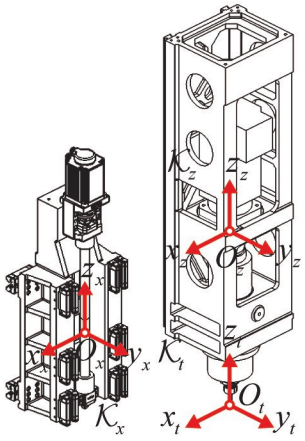	$\mathbf{R}_x = \mathbf{R}_0\ \mathbf{R}_z = \mathbf{R}_0\ \mathbf{R}_t = \mathbf{R}_0$
Rotary table	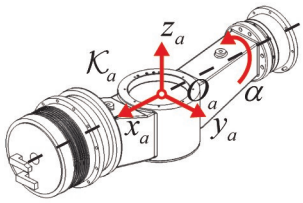	$\mathbf{R}_a = \mathrm{Rot}(x_0, \alpha)\mathbf{R}_0$
Worktable	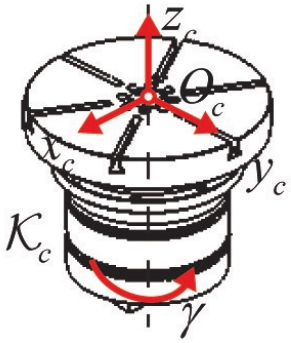	$\mathbf{R}_c = \mathrm{Rot}(x_0, \alpha)\mathrm{Rot}(z_a, \gamma)\mathbf{R}_0$

Note: $\mathrm{Rot}(axis, \theta) \in \mathbb{R}^{3\times3}$ denotes the coordinate axis about which the rotation through θ is performed to obtain the orientation matrix.

3. Position Analysis

3.1. Inverse Position Kinematics

Inverse position kinematics provides an essential basis for multi-axis coordinated motion as well as the subsequent modeling of velocity, acceleration, and rigid-body dynamics of five-axis CNC machine tools. Given the geometric parameters of the machine-tool mechanism and the tool machining-task variable $\mathbf{x}_t^{(w)}$, which consists of the position vector $\mathbf{p}_t^{(w)}$ of the tool reference point expressed in the workpiece coordinate frame $\mathcal{K}_w$ and the unit tool-axis direction vector $\mathbf{n}_t^{(w)}$, the inverse position problem is to determine the positions/angles of the five machine axes, i.e., the unified generalized coordinates $\mathbf{q}$ of the five actuated axes.

The unified generalized coordinates $\mathbf{q}$ of the five actuated axes are defined as

$$\mathbf{q} = \begin{pmatrix} q_X & q_Y & q_Z & q_A & q_C \end{pmatrix}^T \in \mathbb{R}^5 \tag{4}$$

where $q_X q_Y q_Z$ denote the displacements of the X-, Y-, and Z-axis translational joints, respectively, while $q_A q_C$ denote the rotation angles of the A- and C-axis rotary joints, respectively.

The machining-task variable $\mathbf{x}_t^{(w)}$ of the five-axis machine tool is defined as

$$\mathbf{x}_t^{(w)} = \begin{pmatrix} \mathbf{p}_t^{(w)} \\ \mathbf{n}_t^{(w)} \end{pmatrix}, \mathbf{x}_t^{(w)} \in \mathbb{R}^3 \times S^2 \tag{5}$$

$$\mathbf{p}_t^{(w)} = \begin{pmatrix} x_t^{(w)} & y_t^{(w)} & z_t^{(w)} \end{pmatrix}^T, \mathbf{n}_t^{(w)} = \begin{pmatrix} I_t^{(w)} & J_t^{(w)} & K_t^{(w)} \end{pmatrix}^T$$

where $\mathbf{x}_t^{(w)}$ denotes the unified machining-task variable of the tool relative to the workpiece, $\mathbf{p}_t^{(w)}$ denotes the position vector of the tool-tip reference point P_t with respect to the workpiece coordinate frame, and $\mathbf{n}_t^{(w)}$ denotes the unit vector along the machining direction of the tool axis. The quantities $x_t^{(w)} y_t^{(w)} z_t^{(w)}$ are the coordinate components of $\mathbf{p}_t^{(w)}$ along the $x_w y_w z_w$ axes of the workpiece coordinate frame, respectively, while $I_t^{(w)}, J_t^{(w)}, K_t^{(w)}$ are the direction cosines of $\mathbf{n}_t^{(w)}$ along the $x_w y_w z_w$ axes, respectively. Since $\mathbf{n}_t^{(w)}$ is constrained to lie on the unit sphere, it satisfies

$$\left(\mathbf{n}_t^{(w)}\right)^T \mathbf{n}_t^{(w)} = 1 \tag{6}$$

The inverse position problem can therefore be formulated as follows: given a target machining task, $\mathbf{x}_t^{(w)}$, satisfying the prescribed constraint equation, determine the five-axis generalized coordinates $\mathbf{x}_t^{(w)}$, subject to the mechanical travel limits, allowable rotary-axis ranges, and trajectory-continuity requirements. Following the screw-coordinate and POE representation of serial machine-tool kinematics [4], the unit motion screws S_X, S_Y, and S_Z of the X-, Y-, and Z-axis translational joints, respectively, are given by

$$\mathbf{S}_X = \left(\mathbf{e}_x^T, \mathbf{0}^T\right)^T, \mathbf{S}_Y = \left(\mathbf{e}_y^T, \mathbf{0}^T\right)^T, \mathbf{S}_Z = \left(\mathbf{e}_z^T, \mathbf{0}^T\right)^T \tag{7}$$

$$\mathbf{e}_x = \begin{pmatrix} 1 & 0 & 0 \end{pmatrix}^T, \mathbf{e}_y = \begin{pmatrix} 0 & 1 & 0 \end{pmatrix}^T, \mathbf{e}_z = \begin{pmatrix} 0 & 0 & 1 \end{pmatrix}^T$$

where $\mathbf{e}_x$, $\mathbf{e}_y$, and $\mathbf{e}_z$ denote the unit direction vectors of the X-, Y-, and Z-axes, respectively. Since $\hat{\mathbf{s}}_X^2 = \mathbf{0}$, $\hat{\mathbf{s}}_Y^2 = \mathbf{0}$, and $\hat{\mathbf{s}}_Z^2 = \mathbf{0}$, their exponential mappings can be written as

$$\mathbf{e}^{\hat{\mathbf{S}}_X q_X} = \begin{bmatrix} \mathbf{I}_3 & q_X \mathbf{e}_x \\ \mathbf{0}^T & 1 \end{bmatrix}, \mathbf{e}^{\hat{\mathbf{S}}_Y q_Y} = \begin{bmatrix} \mathbf{I}_3 & q_Y \mathbf{e}_y \\ \mathbf{0}^T & 1 \end{bmatrix}, \mathbf{e}^{\hat{\mathbf{S}}_z q_z} = \begin{bmatrix} \mathbf{I}_3 & q_Z \mathbf{e}_z \\ \mathbf{0}^T & 1 \end{bmatrix} \tag{8}$$

Therefore, the product of the three translational motion screws can be expressed as

$$\mathbf{e}^{\hat{\mathbf{S}}_Y q_Y} \mathbf{e}^{\hat{\mathbf{S}}_X q_X} \mathbf{e}^{\hat{\mathbf{S}}_Z q_Z} = \begin{bmatrix} \mathbf{I}_3 & \mathbf{d} \\ \mathbf{0}^T & 1 \end{bmatrix} \tag{9}$$

$$\mathbf{d} = \begin{pmatrix} q_X & q_Y & q_z \end{pmatrix}^T$$

where $\mathbf{d}$ denotes the displacement vector formed by the three translational axes.

The tool-side POE is given by

$$\mathbf{g}_t^{(0)} = \mathbf{e}^{\hat{\mathbf{S}}_Y q_Y} \, \mathbf{e}^{\hat{\mathbf{S}}_X q_X} \, \mathbf{e}^{\hat{\mathbf{S}}_Z q_Z} \mathbf{M}_t \tag{10}$$

$$\mathbf{M}_t = \begin{bmatrix} \mathbf{I}_3 & \mathbf{p}_{t0}^{(0)} \\ \mathbf{0}^T & 1 \end{bmatrix}$$

where $\mathbf{g}_t^{(0)}$ denotes the homogeneous pose of the tool coordinate frame with respect to the machine-bed coordinate frame, $\mathbf{M}_t$ denotes the zero-configuration homogeneous transformation matrix of the tool-side kinematic chain, and $\mathbf{p}_{t0}^{(0)}$ denotes the position vector of the origin of the tool coordinate frame at the zero configuration, expressed in the machine-bed coordinate frame. Substituting Equation (9) into Equation (10) gives

$$\mathbf{g}_t^{(0)} = \begin{bmatrix} \mathbf{I}_3 & \mathbf{p}_{t0}^{(0)} + \mathbf{d} \\ \mathbf{0}^T & 1 \end{bmatrix} \tag{11}$$

Equation (11) shows that, although the three XYZ joints are retained in the unified formulation as three motion screws, the rotational submatrices of their exponential mappings remain equal to $\mathbf{I}_3$ because all of their angular-velocity components are zero.

The unit motion screws $\mathbf{S}_A$ and $\mathbf{S}_C$ of the A- and C-axis rotary joints, respectively, are given by

$$\mathbf{S}_A = \left(\mathbf{0}^T, \mathbf{e}_x^T\right)^T, \mathbf{S}_C = \left(\mathbf{0}^T, \mathbf{e}_z^T\right)^T \tag{12}$$

According to the Rodrigues exponential formula used in the exponential-coordinate representation of rigid-body rotations [4],

$$\begin{aligned} \mathbf{e}^{[\mathbf{e}_x\times]q_A} &= \mathbf{I}_3 + \sin q_A[\mathbf{e}_x\times] + (1-\cos q_A)[\mathbf{e}_x\times]^2 = \mathbf{R}_x(q_A) \\ \mathbf{e}^{[\mathbf{e}_z\times]q_C} &= \mathbf{I}_3 + \sin q_C[\mathbf{e}_z\times] + (1-\cos q_C)[\mathbf{e}_z\times]^2 = \mathbf{R}_z(q_C) \end{aligned} \tag{13}$$

which gives

$$\mathbf{e}^{\hat{\mathbf{S}}_A q_A} = \begin{bmatrix} \mathbf{R}_x(q_A) & \mathbf{0} \\ \mathbf{0}^T & 1 \end{bmatrix}, \mathbf{e}^{\hat{\mathbf{S}}_C q_C} = \begin{bmatrix} \mathbf{R}_z(q_C) & \mathbf{0} \\ \mathbf{0}^T & 1 \end{bmatrix} \tag{14}$$

The workpiece-side rotation matrix is defined as

$$\mathbf{R}_w = \mathbf{R}_x(q_A)\mathbf{R}_z(q_C) \tag{15}$$

where $\mathbf{R}_w$ denotes the rotation matrix of the AC rotary chain with respect to the machine-bed coordinate frame. Substituting it into the workpiece-side POE formulation yields

$$\mathbf{g}_w^{(0)} = \mathbf{e}^{\hat{\mathbf{S}}_A q_A}\mathbf{e}^{\hat{\mathbf{S}}_C q_C}\mathbf{M}_w \tag{16}$$

$$\mathbf{M}_w = \begin{bmatrix} \mathbf{I}_3 & \mathbf{p}_{w0}^{(0)} \\ \mathbf{0}^T & 1 \end{bmatrix}$$

where $\mathbf{g}_w^{(0)}$ denotes the homogeneous pose of the workpiece coordinate frame with respect to the machine-bed coordinate frame, and $\mathbf{p}_{w0}^{(0)}$ denotes the position vector of the origin of the workpiece coordinate frame at the zero configuration, expressed in the machine-bed coordinate frame. Substituting Equation (14) into Equation (16) yields

$$\mathbf{g}_w^{(0)} = \begin{bmatrix} \mathbf{R}_w & \mathbf{R}_w\mathbf{p}_{w0}^{(0)} \\ \mathbf{0}^T & 1 \end{bmatrix} \tag{17}$$

The pose of the tool relative to the workpiece is given by

$$\mathbf{g}_t^{(v)} = \left(\mathbf{g}_w^{(0)}\right)^{-1}\mathbf{g}_t^{(0)} \tag{18}$$

$$\left(\mathbf{g}_w^{(0)}\right)^{-1} = \begin{bmatrix} \mathbf{R}_w^T & -\mathbf{R}_w^T\left(\mathbf{R}_w\mathbf{p}_{w0}^{(0)}\right) \\ \mathbf{0}^T & 1 \end{bmatrix} = \begin{bmatrix} \mathbf{R}_w^T & -\mathbf{p}_{w0}^{(0)} \\ \mathbf{0}^T & 1 \end{bmatrix}$$

where $\mathbf{g}_t^{(w)}$ denotes the homogeneous pose of the tool coordinate frame with respect to the workpiece coordinate frame. Substituting Equations (10) and (17) into Equation (18) gives

$$\mathbf{g}_t^{(w)} = \begin{bmatrix} \mathbf{R}_w^T & \mathbf{R}_w^T\left(\mathbf{p}_{t0}^{(0)} + \mathbf{d}\right) - \mathbf{p}_{w0}^{(0)} \\ \mathbf{0}^T & 1 \end{bmatrix} \tag{19}$$

According to Equations (15) and (19),

$$\mathbf{R}_t^{(w)} = \mathbf{R}_w^T = \left(\mathbf{R}_x(q_A)\mathbf{R}_z(q_C)\right)^T = \mathbf{R}_z(-q_C)\mathbf{R}_x(-q_A) \tag{20}$$

where $\mathbf{R}_t^{(w)}$ denotes the target orientation matrix of the tool relative to the workpiece. Expanding the above expression gives

$$\mathbf{R}_t^{(w)} = \begin{bmatrix} r_{11} & r_{12} & r_{13} \\ r_{21} & r_{22} & r_{23} \\ r_{31} & r_{32} & r_{33} \end{bmatrix} = \begin{bmatrix} \cos q_C & \sin q_C \cos q_A & \sin q_C \sin q_A \\ -\sin q_C & \cos q_C \cos q_A & \cos q_C \sin q_A \\ 0 & -\sin q_A & \cos q_A \end{bmatrix} \tag{21}$$

The current tool-axis direction is given by

$$\mathbf{n}_t^{(w)} = \mathbf{R}_t^{(w)}\mathbf{n}_{t0} \tag{22}$$

where $\mathbf{n}_t^{(w)}$ denotes the current unit vector of the machining direction of the tool axis, and $\mathbf{n}_{t0}$ denotes the initial tool-axis direction $-\mathbf{e}_z$. Substituting Equation (21) into Equation (22) gives

$$\mathbf{n}_t^{(w)} = \begin{pmatrix} I_t^{(w)} \\ J_t^{(w)} \\ K_t^{(w)} \end{pmatrix} = \begin{pmatrix} -\sin q_C \sin q_A \\ -\cos q_C \sin q_A \\ -\cos q_A \end{pmatrix} \tag{23}$$

To distinguish the two possible solution branches associated with positive and negative values of $\sin q_A$, define

$$\rho_n = \sqrt{\left(I_t^{(w)}\right)^2 + \left(J_t^{(w)}\right)^2}, \sin q_A = \sigma_A \rho_n, \sigma_A \in \{+1, -1\} \tag{24}$$

where ρ_n denotes the magnitude of the projection of the tool-axis direction onto the workpiece $x_w y_w$ plane, and σ_A is the branch indicator for the analytical solution of the A axis, specifying the sign of $\sin q_A$. When the allowable mechanical range of the A-axis rotation is restricted a priori to a single-valued interval, σ_A can be determined directly from that range.

Combining the third relation in Equation (23) with Equation (24), the analytical solution for the A-axis rotation can be written as

$$q_A = \operatorname{atan2}\left(\sigma_A \rho_n, -K_t^{(w)}\right) \tag{25}$$

When $\rho_n \neq 0$, the first two relations in Equation (23), together with Equation (24), give

$$q_C = \operatorname{atan2}\left(-\sigma_A I_t^{(w)}, -\sigma_A J_t^{(w)}\right) \tag{26}$$

When $\rho_n = \sqrt{\left(I_t^{(w)}\right)^2 + \left(J_t^{(w)}\right)^2} = 0$, it follows that $I_t^{(w)} = J_t^{(w)} = 0$, indicating that the tool axis is parallel or antiparallel to the workpiece z_w axis. In this case, the tool-axis direction alone cannot distinguish a rotation about the current tool-axis direction. When $K_t^{(w)} = +1$, the equivalent solutions $q_A = \pm\pi$ consistent with the allowable mechanical range are obtained. At such configurations, the C-axis angle should be selected continuously according to the preceding trajectory sample, a prescribed reference angle, or a minimum-axis-motion criterion, rather than being determined independently from the tool-axis direction alone.

Once the A- and C-axis angles have been determined from Equations (25) and (26), Equation (21) gives the finite orientation matrix consistent with the target tool-axis direction. Substituting the target tool-tip position $\mathbf{p}_{t,d}^{(w)}$ into the translational subblock of Equation (19) gives

$$\mathbf{p}_{t,d}^{(w)} + \mathbf{p}_{w0}^{(0)} = \mathbf{R}_t^{(w)}\left(\mathbf{p}_{t0}^{(0)} + \mathbf{d}\right) \tag{27}$$

Premultiplying both sides of Equation (27) by $\left(\mathbf{R}_w^T\right)^T$ yields

$$\mathbf{d} = \left(\mathbf{R}_t^{(w)}\right)^T\left(\mathbf{p}_{t,d}^{(w)} + \mathbf{p}_{w0}^{(0)}\right) - \mathbf{p}_{t0}^{(0)} \tag{28}$$

$$q_X = \mathbf{e}_x^T\mathbf{d}, q_Y = \mathbf{e}_y^T\mathbf{d}, q_Z = \mathbf{e}_z^T\mathbf{d}$$

3.2. Forward Position Kinematics

The forward position kinematics of a five-axis CNC machine tool provides an essential theoretical basis for motion control and workspace-boundary analysis. Given the geometric parameters of the machine-tool system and the unified generalized coordinates, $\mathbf{q}$, of the five actuated axes, the objective is to determine the tool machining-task variable $\mathbf{x}_t^{(w)}$. Given the positions and angles of the five machine axes, $\mathbf{q} = \begin{pmatrix} q_X & q_Y & q_Z & q_A & q_C \end{pmatrix}^T$, the forward position problem is to determine the tool-tip position $\mathbf{p}_t^{(w)}$ in the workpiece coordinate frame and the machining direction of the tool axis $\mathbf{n}_{t,d}^{(w)}$. The forward- and inverse-position solutions are based on the same two POE kinematic chains, and therefore no additional geometric model is required. From the translational subblock of Equation (19), the forward solution for the tool-tip position $\mathbf{p}_t^{(w)}$ is obtained directly as

$$\mathbf{p}_t^{(w)} = \mathbf{R}_t^{(w)}\left(\mathbf{p}_{t0}^{(0)} + \mathbf{d}\right) - \mathbf{p}_{w0}^{(0)} \tag{29}$$

According to Equation (23), together with the orthogonality of the rotation matrix and the initial tool-axis direction $\mathbf{n}_{t0}$ is $-\mathbf{e}_z$, the tool-axis direction obtained from the forward solution automatically preserves unit magnitude, i.e.,

$$\left(\mathbf{n}_t^{(w)}\right)^T\mathbf{n}_t^{(w)} = \mathbf{n}_{t0}^T\left(\mathbf{R}_t^{(w)}\right)^T\mathbf{R}_t^{(w)}\mathbf{n}_{t0} = \mathbf{n}_{t0}^T\mathbf{n}_{t0} = 1 \tag{30}$$

Combining Equations (29) and (30), the unified machining-task output of the forward position kinematics can be written as

$$\mathbf{x}_t^{(w)} = \begin{pmatrix}\mathbf{p}_t^{(w)} \\ \mathbf{n}_t^{(w)}\end{pmatrix} = \begin{pmatrix}\mathbf{R}_t^{(w)}\left(\mathbf{p}_{t0}^{(0)} + \mathbf{d}\right) - \mathbf{p}_{w0}^{(0)} \\ -\mathbf{R}_t^{(w)}\mathbf{e}_z\end{pmatrix} \tag{31}$$

3.3. Validation of the Forward- and Inverse-Position Kinematic Models of the Five-Axis CNC Machine Tool

To verify the numerical consistency and closed-loop correctness of the developed forward- and inverse-position kinematic models for the XYZAC five-axis CNC machine tool, a closed-loop validation strategy of "inverse kinematics–forward kinematics–inverse kinematics" is adopted. First, a set of continuously varying tool machining-task variables is prescribed in the workpiece coordinate system, including the tool-tip position vector and the unit tool-axis direction vector. The given machining-task variable $\mathbf{x}_t^{(w)}$ is substituted into the proposed inverse position kinematic model to obtain the corresponding unified generalized coordinates of the five active axes, denoted as $\mathbf{q}_{\text{inv}}$. Subsequently, these generalized coordinates are substituted into the developed forward position kinematic model to reconstruct the machining-task variable of the tool relative to the workpiece, denoted as $\hat{\mathbf{x}}_t^{(w)}$.

To enable the validation results to be directly evaluated in the generalized-coordinate space of the five active axes, the reconstructed machining-task variable $\hat{\mathbf{x}}_t^{(w)}$ obtained from the forward kinematic model is further substituted into the same inverse kinematic model, yielding the closed-loop generalized coordinates $\mathbf{q}_{cl}$. Therefore, the entire closed-loop verification process of the forward- and inverse-position kinematics can be expressed as $\mathbf{x}_t^{(w)} \rightarrow \mathbf{q}_{\text{inv}} \rightarrow \hat{\mathbf{x}}_t^{(w)} \rightarrow \mathbf{q}_{\text{cl}}$. If the established forward- and inverse-position kinematic models maintain consistency in the mathematical derivation, coordinate transformations, screw-theoretic exponential mappings, and inverse-solution branch selection, the following condition should be satisfied $\mathbf{q}_{\text{inv}} = \mathbf{q}_{\text{cl}}$.

Figure 2 presents the closed-loop validation results of the forward- and inverse-position kinematics for the five active axes. The solid curves represent the inverse-kinematic solutions directly obtained from the initial tool machining-task variables, whereas the dashed curves denote the closed-loop results obtained through the "inverse kinematics–forward kinematics–inverse kinematics" procedure.

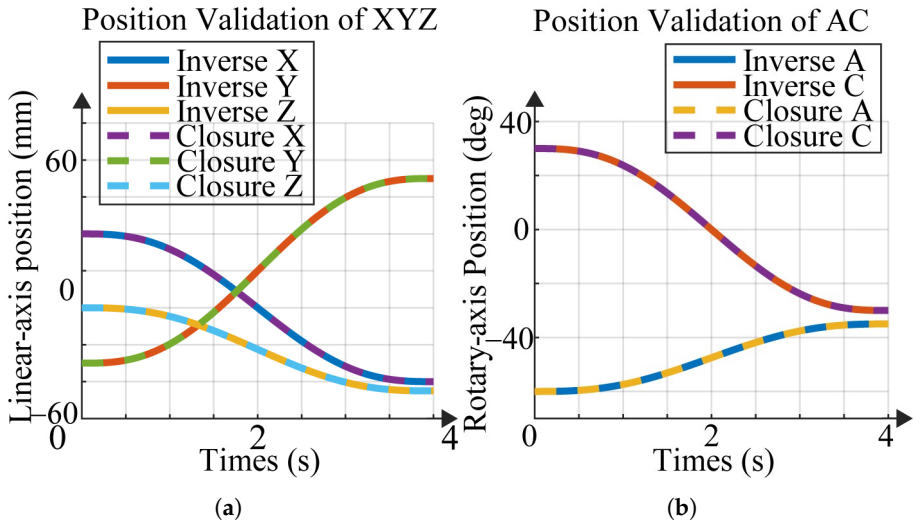

Figure 2. Position forward–inverse kinematic closure validation of the five-axis machine tool: (**a**) XYZ Axis. (**b**) AC Axis.

To quantitatively evaluate the closed-loop consistency of the forward- and inverse-position kinematic models, the generalized-coordinate closure error of the j-th actuated axis is defined as

$$e_{q,j}(k) = q_{j,\text{cl}}(k) - q_{j,\text{inv}}(k), \quad j \in \{X, Y, Z, A, C\} \tag{32}$$

where $q_{j,\mathrm{inv}}(k)$ denotes the generalized coordinate directly obtained from the prescribed machining-task variables through inverse kinematics, $q_{j,\mathrm{cl}}(k)$ denotes the corresponding result obtained through the inverse–forward–inverse closure procedure, k denotes the sampling index, and N is the total number of samples. The root-mean-square error (RMSE) and maximum absolute error (MaxAE) are respectively defined as

$$\mathrm{RMSE}_{q,j} = \sqrt{\frac{1}{N}\sum_{k=1}^{N} e_{q,j}^2(k)}, E_{q,j}^{\max} = \max_{1\le k\le N} |e_{q,j}(k)| \tag{33}$$

The quantitative closure errors are summarized in Table 3. The RMSE of the X-, Y-, and Z-axis translational coordinates are 1.347116×10^{-14}, 2.385889×10^{-14}, and 3.811000×10^{-14} mm, while the maximum absolute errors are 6.938894×10^{-14}, 9.020562×10^{-14}, and 1.110223×10^{-13} mm, respectively. For the A and C rotary axes, the corresponding RMSE values are 2.657723×10^{-15} and 2.019351×10^{-15} deg, while the maximum absolute errors are 1.272222×10^{-14} and 6.361109×10^{-15} deg, respectively. These quantitative results confirm that the generalized coordinates reconstructed through the inverse–forward–inverse procedure remain consistent with the original inverse-kinematic solutions over the investigated trajectory. No branch switching or discontinuity is observed within the selected reachable machining range, thereby validating the numerical closed-loop consistency of the developed forward- and inverse-position kinematic models. The residual errors remain close to numerical round-off precision.

Table 3. Positioning error evaluation results.

Axis	RMSE	Standard Deviation	Maximum Absolute Error
X	1.347116×10^{-14} mm	1.348251×10^{-14} mm	6.938894×10^{-14} mm
Y	2.385889×10^{-14} mm	2.385854×10^{-14} mm	9.020562×10^{-14} mm
Z	3.811000×10^{-14} mm	3.814527×10^{-14} mm	1.110223×10^{-13} mm
A	2.657723×10^{-15} deg	2.658008×10^{-15} deg	1.272222×10^{-14} deg
C	2.019351×10^{-15} deg	2.014525×10^{-15} deg	6.361109×10^{-15} deg

The present validation has a different emphasis from the generalized kinematic and tool-path studies in Refs. [4,8,9]. Yang and Altintas [4] experimentally verified generalized inverse kinematics and singularity-avoiding tool-path generation, My and Bohez [8] focused on differential-kinematic performance indices for different machine configurations, whereas Lu et al. [9] evaluated the smoothness of rotary-axis motion under SO(3)-based orientation processing. In contrast, the present closure test specifically examines the consistency of the representation interfaces $\mathbf{x}_t^{(w)} \to \mathbf{q} \to \hat{\mathbf{x}}_t^{(w)} \to \mathbf{q}_{\mathrm{cl}}$. Therefore, the validation is complementary to, the trajectory-performance and singularity-avoidance validations reported in the literature.

4. Screw-Based Differential Kinematic and Rigid-Body Dynamic Modeling

4.1. Inverse Velocity Modeling

As shown in Figure 1b, the inverse velocity analysis of the five-axis CNC machine tool is performed based on the known geometric parameters of the machine-tool mechanism, the prescribed tool machining-task variable $\mathbf{x}_t^{(w)}$, and the first-order motion variable $\dot{\mathbf{x}}_t^{(w)}$ in the machining-task space. The latter consists of the actual linear velocity $\mathbf{v}_t^{(w)}$ of the tool reference point relative to the workpiece and the first-order time derivative $\dot{\mathbf{n}}_t^{(w)}$ of the unit tool-axis direction vector. The objective is to determine the translational and angular velocities of the five machine axes, i.e., the unified generalized velocity $\dot{\mathbf{q}}$ of the five actuated axes. The generalized velocity $\dot{\mathbf{q}}$ of the five actuated axes is defined as

$$\dot{\mathbf{q}} = (\dot{q}_X \quad \dot{q}_Y \quad \dot{q}_Z \quad \dot{q}_A \quad \dot{q}_C)^T \in \mathbb{R}^5 \tag{34}$$

where $\dot{q}_X\dot{q}_Y\dot{q}_Z$ denote the velocities of the X-, Y-, and Z-axis translational joints, respectively, while $\dot{q}_A\dot{q}_C$ denote the angular velocities of the A- and C-axis rotary joints, respectively.

The first-order motion variable $\dot{\mathbf{x}}_t^{(w)}$ in the machining-task space of the five-axis machine tool is defined as

$$\dot{\mathbf{x}}_t^{(w)} = \begin{pmatrix} \mathbf{v}_t^{(w)} \\ \dot{\mathbf{n}}_t^{(w)} \end{pmatrix} \tag{35}$$

$$\mathbf{v}_t^{(w)} = \begin{pmatrix} v_{x,t}^{(w)} & v_{y,t}^{(w)} & v_{z,t}^{(w)} \end{pmatrix}^T, \dot{\mathbf{n}}_t^{(w)} = \begin{pmatrix} \dot{I}_t^{(w)} & \dot{J}_t^{(w)} & \dot{K}_t^{(w)} \end{pmatrix}^T$$

where $\dot{\mathbf{x}}_t^{(w)}$ denotes the first-order time derivative of the machining-task variable, $\mathbf{v}_t^{(w)}$ denotes the actual linear velocity of the tool reference point relative to the workpiece, and $\dot{\mathbf{n}}_t^{(w)}$ denotes the first-order time derivative of the unit tool-axis direction vector expressed in the fixed workpiece coordinate basis. Since the tool-axis direction is subject to the unit-sphere constraint, differentiating Equation (6) with respect to time gives

$$\left(\mathbf{n}_t^{(w)}\right)^T \dot{\mathbf{n}}_t^{(w)} = 0 \tag{36}$$

The first-order motion variable $\dot{\mathbf{x}}_t^{(w)}$ in the machining-task space of the current five-axis machine tool is not a standard rigid-body motion screw. The physical quantity describing the instantaneous rotation of a rigid body is the actual spatial angular-velocity vector $\boldsymbol{\omega}_t^{(w)}$. For the tool-axis direction rigidly attached to the tool body, the fundamental rigid-body kinematic relation is

$$\dot{\mathbf{n}}_t^{(w)} = \boldsymbol{\omega}_t^{(w)} \times \mathbf{n}_t^{(w)} = -[\mathbf{n}_t^{(w)}\times]\boldsymbol{\omega}_t^{(w)} \tag{37}$$

Moreover,

$$\operatorname{rank}[\mathbf{n}_t^{(w)}\times] = 2, [\mathbf{n}_t^{(w)}\times]\mathbf{n}_t^{(w)} = \mathbf{0} \tag{38}$$

Therefore, $\mathbf{n}_t^{(w)}$ and $\dot{\mathbf{n}}_t^{(w)}$ can directly determine only the component of the actual spatial angular velocity perpendicular to the tool axis, whereas the angular-velocity component along the tool-axis direction cannot be determined from these two quantities alone.

However, the system considered here is not a general rigid body with three rotational degrees of freedom. For the XYZAC five-axis machine tool investigated in this study, and within the kinematic formulation that does not introduce an additional generalized coordinate for spindle rotation, the orientation motion of the tool relative to the workpiece is jointly governed by the two active rotary degrees of freedom, A and C. Therefore, the allowable angular-motion subspace defined by the current POE model can be used to determine, within the mechanism-constrained subspace, the actual spatial angular velocity consistent with the prescribed variation of the tool-axis direction.

Define the rotary-joint subvector as

$$\boldsymbol{\eta}_{AC} = \begin{pmatrix} q_A & q_C \end{pmatrix}^T, \dot{\boldsymbol{\eta}}_{AC} = \begin{pmatrix} \dot{q}_A & \dot{q}_C \end{pmatrix}^T \tag{39}$$

Once the current finite configuration $\mathbf{q}$ is determined from the inverse position solution, the allowable angular-motion matrix is constructed, following the general POE screw-based velocity formulation, from the angular-velocity components of the current unit allowable motion screws associated with the A and C rotary axes,

$$\mathbf{U}_t^{(w)} = \begin{bmatrix} \mathbf{u}_A^{(w)} & \mathbf{u}_C^{(w)} \end{bmatrix} \in \mathbb{R}^{3\times 2} \tag{40}$$

$$\mathbf{u}_A^{(w)} = \mathbf{R}_z(-q_C)\mathbf{e}_x^{(w)}, \mathbf{u}_C^{(w)} = \mathbf{e}_z^{(w)}$$

where $\mathbf{U}_t^{(w)}$ denotes the matrix composed of the current unit-axis directions corresponding to the physically positive directions of the A and C rotary axes, expressed in the workpiece coordinate frame. $\mathbf{u}_A^{(w)}$ denotes the unit-axis direction of the positive A-axis motion expressed in the workpiece coordinate frame at the current configuration, and $\mathbf{u}_C^{(w)}$ denotes the corresponding unit-axis direction of the positive C-axis motion. Accordingly, the actual spatial angular velocity of the tool satisfies

$$\boldsymbol{\omega}_t^{(w)} = -\mathbf{U}_t^{(w)}\dot{\boldsymbol{\eta}}_{AC} \tag{41}$$

Substituting Equation (41) into Equation (37) gives

$$\dot{\mathbf{n}}_t^{(w)} = \mathbf{J}_{n,t}^{(w)}\dot{\boldsymbol{\eta}}_{AC} \tag{42}$$

$$\mathbf{J}_{n,t}^{(w)} = [\mathbf{n}_t^{(w)}\times]\mathbf{U}_t^{(w)}$$

where $\mathbf{J}_{n,t}^{(w)}$ denotes the instantaneous mapping matrix from the allowable orientation-motion subspace of the current XYZAC configuration to the tangent space of the unit sphere associated with the tool-axis direction.

To quantitatively characterize the orientation singularity of the proposed task-to-screw mapping, the explicit form of the tool-axis-direction Jacobian is examined. For the current XYZAC configuration, the tool-axis direction and the allowable angular-motion basis can be expressed as

$$\left(\mathbf{J}_{n,t}^{(w)}\right)^T\mathbf{J}_{n,t}^{(w)} = \begin{bmatrix} 1 & 0 \\ 0 & \sin^2 q_A \end{bmatrix} \tag{43}$$

$$\mathbf{J}_{n,t}^{(w)} = \begin{bmatrix} -\cos q_A \sin q_C & -\sin q_A \cos q_C \\ -\cos q_A \cos q_C & \sin q_A \sin q_C \\ \sin q_A & 0 \end{bmatrix}$$

and hence the singular values of $\mathbf{J}_{n,t}^{(w)}$ are

$$\sigma_1 = 1, \quad \sigma_2 = |\sin q_A| \tag{44}$$

Therefore,

$$\operatorname{rank}\left(\mathbf{J}_{n,t}^{(w)}\right) = \begin{cases} 2, & \sin q_A \neq 0 \\ 1, & \sin q_A = 0 \end{cases} \tag{45}$$

Equation (45) explicitly reveals the rank-deficiency mechanism of the task-orientation mapping. As $q_A \to 0$, the second column of $\mathbf{J}_{n,t}^{(w)}$, which represents the sensitivity of the tool-axis direction to the C-axis motion, approaches zero. Physically, the positive C-axis rotation increasingly corresponds to a relative rotation about the instantaneous tool-axis direction and therefore produces vanishing first-order variation of the unit tool-axis vector. For the mechanical range $q_A \in [-120°, 0°)$ considered in this study, the practically relevant singular boundary is $q_A \to 0^-$.

For nonsingular configurations, the 2-norm condition number is

$$\kappa_2\left(\mathbf{J}_{n,t}^{(w)}\right) = \frac{\sigma_{\max}}{\sigma_{\min}} = \frac{1}{|\sin q_A|} \tag{46}$$

whereas the condition number of the corresponding normal matrix is

$$\kappa_2\left[\left(\mathbf{J}_{n,t}^{(w)}\right)^T\mathbf{J}_{n,t}^{(w)}\right]=\frac{1}{\sin^2 q_A} \tag{47}$$

For a perturbation, $\delta\dot{\mathbf{n}}_t^{(w)}$, in the tool-axis-direction rate, the corresponding perturbation in the recovered A/C angular-rate vector satisfies

$$\|\delta\dot{\boldsymbol{\eta}}_{AC}\|_2\le\frac{1}{|\sin q_A|}\left\|\delta\dot{\mathbf{n}}_t^{(w)}\right\|_2 \tag{48}$$

Thus, the numerical degeneration of the inverse mapping is governed directly by the minimum singular value of $\mathbf{J}_{n,t}^{(w)}$. The same conditioning characteristic is inherited by the acceleration-level mapping because the same Jacobian inverse is subsequently involved in recovering the A- and C-axis angular accelerations. It should be emphasized that this degeneration originates from the S^2-based tool-axis-direction representation rather than from physical immobilization of the C axis. At the exact singular configuration, the C-axis state cannot be uniquely recovered from the instantaneous tool-axis direction and its derivatives alone; therefore, the trajectory-continuity strategy introduced in the position inverse solution is retained.

Accordingly, for a nonsingular orientation configuration satisfying $\sin q_A\neq 0$, the allowable angular-rate vector can be recovered as

$$\dot{\boldsymbol{\eta}}_{AC}=\left(\mathbf{J}_{n,t}^{(w)}\right)^L\dot{\mathbf{n}}_t^{(w)} \tag{49}$$

$$\left(\mathbf{J}_{n,t}^{(w)}\right)^L=\left[\left(\mathbf{J}_{n,t}^{(w)}\right)^T\mathbf{J}_{n,t}^{(w)}\right]^{-1}\left(\mathbf{J}_{n,t}^{(w)}\right)^T$$

Substituting Equation (49) back into Equation (41) yields

$$\boldsymbol{\omega}_t^{(w)}=\mathbf{L}_{\omega,t}^{(w)}\dot{\mathbf{n}}_t^{(w)} \tag{50}$$

$$\mathbf{L}_{\omega,t}^{(w)}=-\mathbf{U}_t^{(w)}\left(\mathbf{J}_{n,t}^{(w)}\right)^L$$

where $\mathbf{L}_{\omega,t}^{(w)}$ denotes the structure-constrained lifting matrix that maps the tool-axis direction rate to the actual spatial angular velocity.

Accordingly, the six-dimensional actual task velocity $\boldsymbol{v}_t^{(w)}$, referenced at the tool reference point, is constructed. Substituting Equation (50) into Equation (51) gives

$$\boldsymbol{v}_t^{(w)}=\begin{pmatrix}\mathbf{v}_t^{(w)}\\ \boldsymbol{\omega}_t^{(w)}\end{pmatrix}=\mathbf{L}_{v,t}^{(w)}\dot{\mathbf{x}}_t^{(w)} \tag{51}$$

$$\mathbf{L}_{v,t}^{(w)}=\begin{bmatrix}\mathbf{I}_3 & \mathbf{0}_{3\times3}\\ \mathbf{0}_{3\times3} & \mathbf{L}_{\omega,t}^{(w)}\end{bmatrix},\boldsymbol{\omega}_t^{(w)}=\begin{pmatrix}\omega_{x,t}^{(w)} & \omega_{y,t}^{(w)} & \omega_{z,t}^{(w)}\end{pmatrix}^T$$

where $\mathbf{L}_{v,t}^{(w)}$ denotes the structure-preserving transformation matrix from the machining-task velocity variables to the six-dimensional task motion screw, and $\boldsymbol{\omega}_t^{(w)}$ denotes the angular velocity of the tool relative to the workpiece.

To ensure strict Lie-group/Lie-algebra consistency between the velocity model and the finite-pose POE model, the relationship between the standard spatial motion screw naturally arising from POE differentiation and the actual velocity of the tool reference point must first be established. Following the standard spatial differential formulation of POE kinematics and the associated adjoint representation [4,11], for the relative pose $g_t^{(w)}$ between the tool and the workpiece, the standard spatial motion screw is defined as

$$\left[\boldsymbol{v}_{s,t}^{(w)}\right]^{\Lambda} = \dot{\mathbf{g}}_t^{(w)}\left(\mathbf{g}_t^{(w)}\right)^{-1} \tag{52}$$

$$\dot{\boldsymbol{g}}_t^{(w)} = \begin{bmatrix} \dot{\boldsymbol{R}}_t^{(w)} & \dot{\boldsymbol{p}}_t^{(w)} \\ \boldsymbol{\theta}^T & 0 \end{bmatrix}, \left(\boldsymbol{g}_t^{(w)}\right)^{-1} = \begin{bmatrix} \left(\boldsymbol{R}_t^{(w)}\right)^T & -\left(\boldsymbol{R}_t^{(w)}\right)^T \boldsymbol{p}_t^{(w)} \\ \boldsymbol{\theta}^T & 1 \end{bmatrix}$$

where $\boldsymbol{v}_{s,t}^{(w)}$ denotes the standard spatial motion screw of the tool rigid body relative to the workpiece coordinate frame, $\dot{\mathbf{g}}_t^{(w)}$ denotes the first-order time derivative of the tool–workpiece relative homogeneous transformation, $\dot{\mathbf{R}}_t^{(w)}$ denotes the first-order time derivative of the tool orientation matrix expressed in the workpiece coordinate frame, and $\dot{\mathbf{p}}_t^{(w)}$ denotes the first-order time derivative of the position vector of the tool reference point expressed in the workpiece coordinate frame. The standard spatial motion screw $\boldsymbol{v}_{s,t}^{(w)}$ and its hat-operator representation $\left[\boldsymbol{v}_{s,t}^{(w)}\right]^{\Lambda}$ are written as

$$\boldsymbol{v}_{s,t}^{(w)} = \begin{pmatrix} \mathbf{v}_{s,t}^{(w)} \\ \boldsymbol{\omega}_t^{(w)} \end{pmatrix}, \left[\boldsymbol{v}_{s,t}^{(w)}\right]^{\Lambda} = \begin{bmatrix} \left[\boldsymbol{\omega}_t^{(w)}\times\right] & \mathbf{v}_{s,t}^{(w)} \\ \mathbf{0}^T & 0 \end{bmatrix} \tag{53}$$

where $\mathbf{v}_{s,t}^{(w)}$ denotes the three-dimensional linear-velocity component of the standard spatial motion screw, which is not the actual linear velocity of the tool reference point.

Comparing the upper-left rotational subblocks of Equations (52) and (53) gives the relationship between the actual spatial angular velocity of the tool and the derivative of its orientation matrix as

$$\left[\boldsymbol{\omega}_t^{(w)}\times\right] = \dot{\mathbf{R}}_t^{(w)}\left(\mathbf{R}_t^{(w)}\right)^T \tag{54}$$

Similarly, a comparison of the upper-right translational subblocks gives the linear-velocity component of the standard spatial motion screw as

$$\mathbf{v}_{s,t}^{(w)} = \dot{\mathbf{p}}_t^{(w)} - \boldsymbol{\omega}_t^{(w)} \times \mathbf{p}_t^{(w)} \tag{55}$$

Since the inverse velocity model takes the actual linear velocity of the tool reference point as its input, i.e., $\mathbf{v}_t^{(w)} = \dot{\mathbf{p}}_t^{(w)}$, Equation (55) can equivalently be rearranged as

$$\mathbf{v}_t^{(w)} = \mathbf{v}_{s,t}^{(w)} + \boldsymbol{\omega}_t^{(w)} \times \mathbf{p}_t^{(w)} \tag{56}$$

Accordingly, a six-dimensional reference-point transformation matrix from the standard spatial motion screw to the task-velocity screw referenced at the tool reference point can be defined as

$$\mathbf{X}_t^{(w)} = \begin{bmatrix} \mathbf{I}_3 & -\left[\mathbf{p}_t^{(w)}\times\right] \\ \mathbf{0}_{3\times3} & \mathbf{I}_3 \end{bmatrix} \in \mathbb{R}^{6\times6} \tag{57}$$

where $\mathbf{X}_t^{(w)}$ denotes the six-dimensional reference-point transformation matrix from the standard spatial motion screw to the task-velocity screw referenced at the tool reference point. Therefore,

$$\boldsymbol{v}_t^{(w)} = \mathbf{X}_t^{(w)} \boldsymbol{v}_{s,t}^{(w)} \tag{58}$$

To directly differentiate the finite tool–workpiece relative pose at the velocity level, the two physical kinematic chains must first be equivalently reformulated as a five-joint relative virtual screw chain expressed in the same workpiece coordinate frame. The tool-side and workpiece-side POE formulations are, respectively,

$$\mathbf{g}_t^{(0)} = e^{\left[\mathbf{S}_Y^{(0)}\right]q_Y} e^{\left[\mathbf{S}_X^{(0)}\right]q_X} e^{\left[\mathbf{S}_Z^{(0)}\right]q_Z} \mathbf{M}_t^{(0)}$$

$$\mathbf{g}_W^{(0)} = e^{\left[\mathbf{S}_A^{(0)}\right]q_A} e^{\left[\mathbf{S}_C^{(0)}\right]q_C} \mathbf{M}_w^{(0)} \tag{59}$$

where $\mathbf{g}_t^{(0)}$ denotes the current homogeneous pose of the tool rigid body relative to the machine-bed coordinate frame, $\mathbf{g}_W^{(0)}$ denotes the current homogeneous pose of the workpiece coordinate frame relative to the machine-bed coordinate frame, and $\mathbf{S}_X^{(0)}$, $\mathbf{S}_Y^{(0)}$, $\mathbf{S}_Z^{(0)}$, $\mathbf{S}_A^{(0)}$, and $\mathbf{S}_C^{(0)}$ denote the zero-configuration unit motion screws of the XYZ actuated axes and the zero-configuration unit rotary motion screws of the AC actuated axes, respectively. Accordingly, the finite pose of the tool relative to the workpiece is first defined by the relative transformation between the two physical kinematic chains as

$$\mathbf{g}_t^{(w)} = \left(\mathbf{g}_w^{(0)}\right)^{-1} \mathbf{g}_t^{(0)} \tag{60}$$

Substituting the tool-side and workpiece-side POE formulations into Equation (60), and using the order-reversal property of the inverse of a matrix product, gives

$$\mathbf{g}_t^{(w)} = \left(\mathbf{M}_w^{(0)}\right)^{-1} e^{-\left[\mathbf{S}_C^{(0)}\right]q_C} e^{-\left[\mathbf{S}_A^{(0)}\right]q_A} e^{\left[\mathbf{S}_Y^{(0)}\right]q_Y} e^{\left[\mathbf{S}_X^{(0)}\right]q_X} e^{\left[\mathbf{S}_Z^{(0)}\right]q_Z} \mathbf{M}_t^{(0)} \tag{61}$$

Using the conjugation identity between homogeneous transformations and matrix exponentials, $\left(\mathbf{M}_w^{(0)}\right)^{-1}$ can be successively shifted to the right, yielding

$$\mathbf{g}_t^{(w)} = \prod_{j=1}^{5} \mathbf{e}^{\hat{\mathbf{\Sigma}}_j^{(w)}\boldsymbol{\theta}_j} \mathbf{M}_t^{(w)} \tag{62}$$

$$\boldsymbol{M}_t^{(w)} = \left(\boldsymbol{M}_w^{(0)}\right)^{-1} \boldsymbol{M}_t^{(0)}, \boldsymbol{\theta} = \begin{pmatrix} q_C & q_A & q_Y & q_X & q_Z \end{pmatrix}^T, \mathbf{\Sigma}_1 = -\mathrm{Ad}_{\left(\boldsymbol{M}_w^{(0)}\right)^{-1}} \mathbf{S}_C^{(0)},$$

$$\mathbf{\Sigma}_2 = -\mathrm{Ad}_{\left(\mathbf{M}_w^{(0)}\right)^{-1}} \mathbf{S}_A^{(0)}, \mathbf{\Sigma}_3 = \mathrm{Ad}_{\left(\mathbf{M}_w^{(0)}\right)^{-1}} \mathbf{S}_Y^{(0)},$$

$$\mathbf{\Sigma}_4 = \mathrm{Ad}_{\left(\mathbf{M}_w^{(0)}\right)^{-1}} \mathbf{S}_X^{(0)}, \mathbf{\Sigma}_5 = \mathrm{Ad}_{\left(\mathbf{M}_w^{(0)}\right)^{-1}} \mathbf{S}_Z^{(0)}, \mathrm{Ad}_{\left(M_w^{(0)}\right)^{-1}} = \begin{bmatrix} \mathbf{I}_3 & -[\mathbf{p}_w^{(0)}]_x \\ \mathbf{0}_{3\times 3} & \mathbf{I}_3 \end{bmatrix}$$

where $\hat{\mathbf{\Sigma}}_j^{(w)}$ denotes the zero-configuration unit motion screw of the jth joint in the unified relative virtual chain, $\boldsymbol{\theta}_j$ denotes the internal joint-coordinate vector arranged according to the actual order of the exponential factors in the relative POE formulation, $\mathbf{M}_t^{(w)}$ denotes the constant homogeneous transformation of the tool rigid body relative to the workpiece coordinate frame when all five axes are at their zero configurations, and $\mathrm{Ad}_{\left(\mathbf{M}_w^{(0)}\right)^{-1}}$ denotes the six-dimensional adjoint transformation matrix for motion screws induced by the pose $\left(\mathbf{M}_w^{(0)}\right)^{-1}$. Although $\mathbf{q}$ and $\boldsymbol{\theta}$ contain the same joint variables, their orderings differ. Therefore, the permutation matrix $\mathbf{E}_q^\theta$ is introduced, such that

$$\boldsymbol{\theta} = \mathbf{E}_q^\theta \mathbf{q} \tag{63}$$

$$\mathbf{E}_q^\theta = \begin{bmatrix} 0 & 0 & 0 & 0 & 1 \\ 0 & 0 & 0 & 1 & 0 \\ 0 & 1 & 0 & 0 & 0 \\ 1 & 0 & 0 & 0 & 0 \\ 0 & 0 & 1 & 0 & 0 \end{bmatrix}$$

According to the spatial differential formula of the POE representation, the instantaneous spatial unit motion screw generated by the kth joint at the current configuration is

$$\boldsymbol{\xi}_{\theta,1}^{(w)} = \boldsymbol{\Sigma}_1, \boldsymbol{\xi}_{\theta,k}^{(w)} = \mathrm{Ad}_{\mathbf{g}_{k-1}^{(w)}} \boldsymbol{\Sigma}_k, k = 2, \ldots, 5 \tag{64}$$

$$\mathbf{g}_{k-1}^{(w)} = \prod_{j=1}^{k-1} \mathbf{e}^{\hat{\boldsymbol{\Sigma}}_j^{(w)} \boldsymbol{\theta}_j}$$

where $\boldsymbol{\xi}_{\theta,k}^{(w)}$ denotes the spatial unit motion screw generated on the tool rigid body, expressed in the workpiece coordinate frame, by the kth actuated axis in the internal POE sequence at the current configuration. Accordingly, the spatial screw Jacobian $\mathbf{J}_{\theta,s,t}^{(w)}$, constructed according to the kinematic-chain ordering $\boldsymbol{\theta} = \begin{pmatrix} q_C & q_A & q_Y & q_X & q_Z \end{pmatrix}^T$, is given by

$$\mathbf{J}_{\theta,s,t}^{(w)} = [\boldsymbol{\xi}_{\theta,1}^{(w)} \quad \boldsymbol{\xi}_{\theta,2}^{(w)} \quad \boldsymbol{\xi}_{\theta,3}^{(w)} \quad \boldsymbol{\xi}_{\theta,4}^{(w)} \quad \boldsymbol{\xi}_{\theta,5}^{(w)}] \in \mathbb{R}^{6\times5} \tag{65}$$

Therefore, the standard spatial motion screw and the internal joint velocities satisfy

$$\boldsymbol{v}_{s,t}^{(w)} = \mathbf{J}_{\theta,s,t}^{(w)} \dot{\boldsymbol{\theta}} \tag{66}$$

$$\dot{\boldsymbol{\theta}} = \mathbf{E}_q^{\theta} \dot{\mathbf{q}}$$

It follows that the spatial screw Jacobian $\mathbf{J}_{s,t}^{(w)}$ arranged according to $\mathbf{q} = (q_X \; q_Y \; q_Z \; q_A \; q_C)^T$ satisfies

$$\boldsymbol{v}_{s,t}^{(w)} = \mathbf{J}_{s,t}^{(w)} \dot{\mathbf{q}} \tag{67}$$

$$\mathbf{J}_{s,t}^{(w)} = \mathbf{J}_{\theta,s,t}^{(w)} \mathbf{E}_q^{\theta}$$

Combining Equations (58) and (67) eliminates the standard spatial motion screw as an intermediate theoretical quantity. This directly yields the unified first-order velocity equation consistent with the input variables of the inverse velocity model in this section,

$$\boldsymbol{v}_t^{(w)} = \mathbf{T}_t^{(w)} \dot{\mathbf{q}} \tag{68}$$

$$\mathbf{T}_t^{(w)} = \mathbf{X}_t^{(w)} \mathbf{J}_{s,t}^{(w)} \in \mathbb{R}^{6\times5}, \quad \mathbf{T}_t^{(w)} = \begin{bmatrix} \mathbf{S}_{X,t}^{(w)} & \mathbf{S}_{Y,t}^{(w)} & \mathbf{S}_{Z,t}^{(w)} & \mathbf{S}_{A,t}^{(w)} & \mathbf{S}_{C,t}^{(w)} \end{bmatrix}$$

where $\mathbf{T}_t^{(w)}$ denotes the unified allowable motion-screw matrix associated with the five actuated axes and referenced at the tool reference point in the workpiece coordinate frame. $\mathbf{S}_{X,t}^{(w)}, \mathbf{S}_{Y,t}^{(w)}, \mathbf{S}_{Z,t}^{(w)}, \mathbf{S}_{A,t}^{(w)} \mathbf{S}_{C,t}^{(w)}$ denote the six-dimensional allowable motion screws generated at the tool reference point, expressed in the workpiece coordinate frame, by unit velocities of the X-, Y-, Z-, A-, and C-axis actuators, respectively.

Because $\mathbf{T}_t^{(w)}$ is a 6×5 matrix, the generalized velocity cannot be obtained by direct inversion. To preserve the physical meaning of screw reciprocity, a unit supplementary constrained motion screw that is linearly independent of the five allowable motion screws is introduced to construct a complete six-dimensional motion-screw basis.

Since the tool-side XYZ chain produces no rotational motion and spindle rotation associated with the cutting process is not considered in this section, the orientation of the tool rigid body relative to the machine bed remains fixed. Therefore, the orientation of the tool relative to the workpiece is

$$\mathbf{R}_t^{(w)} = \mathbf{R}_z(-q_C)\mathbf{R}_x(-q_A) \tag{69}$$

Because the tool-side XYZ axes remain parallel to the tool coordinate frame, the three unit translational directions are assembled in the XYZ order as

$$\mathbf{D}_t^{(w)} = \begin{bmatrix} d_{X,t}^{(w)} & d_{Y,t}^{(w)} & d_{Z,t}^{(w)} \end{bmatrix} = \mathbf{R}_t^{(w)} \tag{70}$$

$$\mathbf{d}_{X,t}^{(w)} = \mathbf{R}_t^{(w)}\mathbf{e}_x^{(t)}, \quad \mathbf{d}_{Y,t}^{(w)} = \mathbf{R}_t^{(w)}\mathbf{e}_y^{(t)}, \quad \mathbf{d}_{Z,t}^{(w)} = \mathbf{R}_t^{(w)}\mathbf{e}_z^{(t)}$$

where $\mathbf{D}_t^{(w)}$ denotes the direction matrix composed of the current unit translational directions of the X-, Y-, and Z-axis actuators expressed in the workpiece coordinate frame, while $\mathbf{d}_{X,t}^{(w)}, \mathbf{d}_{Y,t}^{(w)}, \mathbf{d}_{Z,t}^{(w)}$ denote the direction vectors at the tool reference point corresponding to unit positive translations of the X-, Y-, and Z-axis actuators, respectively, expressed in the workpiece coordinate frame.

Because the tool–workpiece relative pose is formulated using the inverse transformation of the workpiece-side kinematic chain, positive q_A and q_C contribute to the instantaneous angular motion of the tool relative to the workpiece along the directions $-\mathbf{u}_A^{(w)}$ and $-\mathbf{u}_C^{(w)}$, respectively. Let P_A and P_C be arbitrary known points on the A- and C-axis lines, with position vectors $\mathbf{c}_A^{(w)}$ and $\mathbf{c}_C^{(w)}$, respectively. The vectors from the corresponding axis reference points to the tool reference point are defined as

$$\mathbf{r}_{A,t}^{(w)} = \mathbf{p}_t^{(w)} - \mathbf{c}_A^{(w)}, \quad \mathbf{r}_{C,t}^{(w)} = \mathbf{p}_t^{(w)} - \mathbf{c}_C^{(w)} \tag{71}$$

where $\mathbf{r}_{A,t}^{(w)}$ and $\mathbf{r}_{C,t}^{(w)}$ denote the position vectors, expressed in the workpiece coordinate frame, from the reference points P_A and P_C on the A- and C-axis lines to the tool reference point P_t. Since unit positive q_A and q_C produce relative angular velocities of $-\mathbf{u}_A^{(w)}$ and $-\mathbf{u}_C^{(w)}$, respectively, the corresponding unit linear-velocity components at P_t are

$$\mathbf{A}_{t0}^{(w)} = \begin{bmatrix} \mathbf{a}_{A,t}^{(w)} & \mathbf{a}_{C,t}^{(w)} \end{bmatrix} \tag{72}$$

$$\mathbf{a}_{A,t}^{(w)} = \mathbf{r}_{A,t}^{(w)} \times \mathbf{u}_A^{(w)} = \left[\mathbf{r}_{A,t}^{(w)}\times\right]\mathbf{u}_A^{(w)}, \quad \mathbf{a}_{C,t}^{(w)} = \mathbf{r}_{C,t}^{(w)} \times \mathbf{u}_C^{(w)} = \left[\mathbf{r}_{C,t}^{(w)}\times\right]\mathbf{u}_C^{(w)}$$

where $\mathbf{A}_{t0}^{(w)}$ denotes the 3×2 matrix composed of the unit relative linear-velocity components generated at the tool reference point P_t by the A and C rotary axes, expressed in the workpiece coordinate frame. $\mathbf{a}_{A,t}^{(w)}$ and $\mathbf{a}_{C,t}^{(w)}$ denote the relative linear-velocity components generated at the tool reference point by the inverse motion of the workpiece-side chain when the A and C actuated axes move with unit positive angular velocities, respectively.

For the current XYZAC architecture, $\mathbf{R}_t^{(w)}$ is a rotation matrix, and the directions of the A and C axes remain unit and mutually orthogonal. Hence,

$$\left(\mathbf{R}_t^{(w)}\right)^T \mathbf{R}_t^{(w)} = \mathbf{I}_3, \left(\mathbf{U}_t^{(w)}\right)^T \mathbf{U}_t^{(w)} = \mathbf{I}_2 \tag{73}$$

A unit constrained angular-motion direction orthogonal to both allowable angular-velocity directions of the A and C axes is defined as

$$\mathbf{n}_{c,t}^{(w)} = \frac{\mathbf{u}_C^{(w)} \times \mathbf{u}_A^{(w)}}{\| \mathbf{u}_C^{(w)} \times \mathbf{u}_A^{(w)} \|}, \| \mathbf{n}_{c,t}^{(w)} \| = 1 \tag{74}$$

where $\mathbf{n}_{c,t}^{(w)}$ denotes the unit constrained angular-motion direction, expressed in the workpiece coordinate frame, that is orthogonal to both allowable relative angular-motion directions associated with the A and C axes.

Since the three XYZ translational axes already span the complete three-dimensional translational subspace, the five-dimensional allowable motion subspace can be completed

to the full six-dimensional motion-screw space by selecting a unit supplementary motion screw passing through the tool reference point P_t and directed along $\mathbf{n}_{c,t}^{(w)}$,

$$\mathbf{S}_{c,t}^{(w)} = \begin{bmatrix} \mathbf{0}_{3\times1} \\ \mathbf{n}_{c,t}^{(w)} \end{bmatrix} \tag{75}$$

where $\mathbf{S}_{c,t}^{(w)}$ denotes the unit constrained motion screw referenced at the tool reference point and expressed in the workpiece coordinate frame, introduced to complete the five-dimensional allowable motion subspace. The five allowable motion screws and the supplementary constrained motion screw are then assembled into a complete motion-screw basis,

$$\bar{\mathbf{T}}_t^{(w)} = \begin{bmatrix} \mathbf{T}_t^{(w)} & \mathbf{S}_{c,t}^{(w)} \end{bmatrix} \in \mathbb{R}^{6\times6} \tag{76}$$

where $\bar{\mathbf{T}}_t^{(w)}$ denotes the complete 6×6 motion-screw basis composed of the five actual allowable motion screws and one supplementary constrained motion screw. Based on the reciprocity between motion screws and wrench screws [12,15,16], the dual wrench-screw basis associated with the complete motion-screw basis is defined as

$$\mathbf{W}_t^{(w)} = \left(\bar{\mathbf{T}}_t^{(w)}\right)^{-T}, \left(\mathbf{W}_t^{(w)}\right)^{T} \bar{\mathbf{T}}_t^{(w)} = \mathbf{I}_6 \tag{77}$$

where $\mathbf{W}_t^{(w)}$ denotes the 6×6 dual wrench-screw basis matrix reciprocal to the complete motion-screw basis in the workpiece coordinate frame. Taking the first five coordinates of the dual basis corresponding to the five actual actuated axes, the selection matrix is defined as

$$\mathbf{E}_a = \begin{bmatrix} \mathbf{I}_5 & \mathbf{0}_{5\times1} \end{bmatrix} \tag{78}$$

where $\mathbf{E}_a$ denotes the 5×6 selection matrix that extracts the velocity coordinates associated with the five actual actuated axes from the complete six-dimensional dual coordinates. Accordingly, in the sense of screw reciprocity,

$$\mathbf{G}_t^{(w)} = \mathbf{E}_a \left(\mathbf{W}_t^{(w)}\right)^{T} \tag{79}$$

where $\mathbf{G}_t^{(w)}$ denotes the 5×6 closed-form analytical left-inverse matrix for the XYZAC topology under the six-dimensional actual task velocity. Premultiplying both sides of Equation (68) by $\mathbf{G}_t^{(w)}$ and using $\mathbf{G}_t^{(w)}\mathbf{T}_t^{(w)} = \mathbf{I}_5$ yields the unified instantaneous first-order analytical inverse solution for the five-axis generalized velocity under the six-dimensional actual task velocity,

$$\dot{\mathbf{q}} = \mathbf{G}_t^{(w)} \boldsymbol{v}_t^{(w)} \tag{80}$$

Substituting Equation (51) into Equation (80) then gives the final inverse velocity solution in terms of the unified machining-task input,

$$\dot{\mathbf{q}} = \mathbf{G}_t^{(w)} \mathbf{L}_{v,t}^{(w)} \dot{\mathbf{x}}_t^{(w)} \tag{81}$$

The main purpose of the above derivation is not to re-establish the basic geometric relationship between the rate of change of the tool-axis direction and the rigid-body angular velocity. Rather, it is to construct a velocity-mapping interface, subject to the kinematic constraints of the target machine tool, between the machining-task space and the rigid-body motion-screw space in view of the different representations used for the five-axis machining-task variables and the rigid-body motion-screw variables. The tool-axis direc-

tion rate $\dot{\mathbf{n}}_t^{(w)}$ contains only two independent directional degrees of freedom in the tangent space of the unit sphere, whereas rigid-body dynamics and the subsequent screw-based differential kinematics require the complete actual spatial angular velocity $\boldsymbol{\omega}_t^{(w)}$. Therefore, the differential relation of the tool-axis direction is coupled with the allowable AC angular-motion subspace generated by the current XYZAC POE model, thereby lifting the machining-task velocity variables to the actual motion screw under the constraints imposed by the mechanism topology.

After completing the transformation from task variables to motion screws, the non-square nature of the allowable motion matrix of the five-axis mechanism is further addressed by introducing a supplementary constrained motion screw that is linearly independent of the five actual allowable motion screws. In this way, the five-dimensional allowable motion subspace is completed to a full six-dimensional motion-screw basis, from which a dual wrench-screw basis is constructed according to motion-screw–wrench-screw reciprocity. This yields an analytical left inverse satisfying $\mathbf{G}_t^{(w)}\mathbf{T}_t^{(w)} = \mathbf{I}_5$ and enables a unified screw-based solution of the instantaneous generalized velocities of the five actuated axes.

Therefore, the principal methodological contribution of this section lies in establishing the two-stage mapping $\dot{\mathbf{x}}_t^{(w)} \rightarrow \boldsymbol{v}_t^{(w)} \rightarrow \dot{\mathbf{q}}$. The proposed factorization is not intended to provide a universally superior numerical alternative to the conventional direct task-Jacobian formulation. Rather, its principal advantages lie in preserving representation consistency between the $\mathbb{R}^3 \times S^2$ machining-task variables and the $se(3)$ rigid-body motion variables, retaining the physical interpretability of the intermediate rigid-body twist, and separating the task-to-screw interface from the generalized-coordinate inversion interface. This structure also enables the second-order effects associated with the variation of the task mapping and the mechanism configuration to be explicitly distinguished in the acceleration model. Moreover, retaining the actual rigid-body twist as an intermediate variable provides a direct and physically consistent interface to the subsequent wrench-based Newton–Euler and virtual-work dynamic formulation. Therefore, the advantage of the proposed two-stage mapping lies primarily in modeling transparency, modularity, and compatibility with the subsequent rigid-body dynamic formulation rather than in an asserted improvement in numerical conditioning or computational efficiency.

4.2. Inverse Acceleration Modeling

As shown in Figure 1b, the inverse acceleration analysis of the five-axis CNC machine tool is performed based on the known geometric parameters of the machine-tool mechanism, the prescribed tool machining-task variable $\mathbf{x}_t^{(w)}$, the first-order motion variable $\dot{\mathbf{x}}_t^{(w)}$ in the machining-task space, and the second-order motion variable $\ddot{\mathbf{x}}_t^{(w)}$ in the machining-task space. The latter consists of the actual linear acceleration $\mathbf{a}_t^{(w)}$ of the tool reference point relative to the workpiece and the second-order time derivative $\ddot{\mathbf{n}}_t^{(w)}$ of the unit tool-axis direction vector. The objective is to determine the linear accelerations of the X-, Y-, and Z-axis translational joints and the angular accelerations of the A- and C-axis rotary joints, i.e., the unified generalized acceleration $\ddot{\mathbf{q}}$ of the five actuated axes.

The generalized acceleration $\ddot{\mathbf{q}}$ of the five actuated axes is defined as

$$\ddot{\mathbf{q}} = \begin{pmatrix} \ddot{q}_X & \ddot{q}_Y & \ddot{q}_Z & \ddot{q}_A & \ddot{q}_C \end{pmatrix}^T \in \mathbb{R}^5 \tag{82}$$

where $\ddot{q}_X, \ddot{q}_Y, \ddot{q}_Z, \ddot{q}_A, \ddot{q}_C$ denote the linear accelerations of the X-, Y-, and Z-axis actuators and the angular accelerations of the A- and C-axis actuators, respectively.

The second-order motion variable $\ddot{\mathbf{x}}_t^{(w)}$ in the machining-task space of the five-axis machine tool is defined as

$$\ddot{\mathbf{x}}_t^{(w)} = \begin{pmatrix} \mathbf{a}_t^{(w)} \\ \ddot{\mathbf{n}}_t^{(w)} \end{pmatrix} \tag{83}$$

$$\mathbf{a}_t^{(w)} = \begin{pmatrix} a_{x,t}^{(w)} & a_{y,t}^{(w)} & a_{z,t}^{(w)} \end{pmatrix}^T, \ddot{\mathbf{n}}_t^{(w)} = \begin{pmatrix} \ddot{I}_t^{(w)} & \ddot{J}_t^{(w)} & \ddot{K}_t^{(w)} \end{pmatrix}^T$$

where $\ddot{\mathbf{x}}_t^{(w)}$ denotes the second-order time derivative of the machining-task variable, $\mathbf{a}_t^{(w)}$ denotes the actual linear acceleration of the tool reference point relative to the workpiece, expressed in the workpiece coordinate frame, and $\ddot{\mathbf{n}}_t^{(w)}$ denotes the second-order time derivative of the unit tool-axis direction vector expressed in the fixed workpiece coordinate basis. Differentiating Equation (36) with respect to time gives

$$(\mathbf{n}_t^{(w)})^T \ddot{\mathbf{n}}_t^{(w)} = -(\dot{\mathbf{n}}_t^{(w)})^T \dot{\mathbf{n}}_t^{(w)} \tag{84}$$

Differentiating Equation (37) with respect to time gives

$$\ddot{\mathbf{n}}_t^{(w)} = \boldsymbol{\alpha}_t^{(w)} \times \mathbf{n}_t^{(w)} + \boldsymbol{\omega}_t^{(w)} \times \dot{\mathbf{n}}_t^{(w)} = -[\mathbf{n}_t^{(w)}\times]\boldsymbol{\alpha}_t^{(w)} + [\boldsymbol{\omega}_t^{(w)}\times]\dot{\mathbf{n}}_t^{(w)} \tag{85}$$

where $\boldsymbol{\alpha}_t^{(w)}$ denotes the actual spatial angular-acceleration vector associated with the instantaneous rotation of the rigid body. Differentiating Equation (41) with respect to time gives

$$\boldsymbol{\alpha}_t^{(w)} = -\dot{\mathbf{U}}_t^{(w)}\dot{\boldsymbol{\eta}} - \mathbf{U}_t^{(w)}\ddot{\boldsymbol{\eta}} \tag{86}$$

$$\ddot{\boldsymbol{\eta}} = \begin{pmatrix} \ddot{q}_A & \ddot{q}_C \end{pmatrix}^T$$

where $\dot{\mathbf{U}}_t^{(w)}$ denotes the first-order time derivative of the allowable angular-motion basis matrix, and $\ddot{\boldsymbol{\eta}}$ denotes the generalized angular acceleration vector of the A and C rotary axes. Even when the generalized angular accelerations of both rotary axes are zero, the allowable rotary-axis directions may still vary with the mechanism configuration, such that

$$\dot{\mathbf{U}}_t^{(w)} \neq \mathbf{0} \tag{87}$$

Substituting Equation (86) into Equation (85) gives

$$\ddot{\mathbf{n}}_t^{(w)} = \mathbf{J}_{n,t}^{(w)}\ddot{\boldsymbol{\eta}} + \mathbf{b}_{n,t}^{(w)} \tag{88}$$

$$\mathbf{b}_{n,t}^{(w)} = [\mathbf{n}_t^{(w)}\times]\dot{\mathbf{U}}_t^{(w)}\dot{\boldsymbol{\eta}} + [\boldsymbol{\omega}_t^{(w)}\times]\dot{\mathbf{n}}_t^{(w)}$$

where $\mathbf{b}_{n,t}^{(w)}$ denotes the velocity-quadratic term in the second-order motion of the tool-axis direction, arising jointly from the configuration-dependent variation of the allowable angular-motion basis and the current angular velocity.

Premultiplying Equation (88) by $\left(\mathbf{J}_{n,t}^{(w)}\right)^L$ gives

$$\ddot{\boldsymbol{\eta}} = \left(\mathbf{J}_{n,t}^{(w)}\right)^L \left(\ddot{\mathbf{n}}_t^{(w)} - \mathbf{b}_{n,t}^{(w)}\right) \tag{89}$$

Substituting Equation (89) back into Equation (86) yields

$$\boldsymbol{\alpha}_t^{(w)} = \mathbf{L}_{\omega,t}^{(w)}\ddot{\mathbf{n}}_t^{(w)} + \mathbf{b}_{\alpha,t}^{(w)} \tag{90}$$

$$\mathbf{b}_{\alpha,t}^{(w)} = -\dot{\mathbf{U}}_t^{(w)}\dot{\boldsymbol{\eta}} - \mathbf{L}_{\omega,t}^{(w)}\mathbf{b}_{n,t}^{(w)}$$

where $\mathbf{b}_{\alpha,t}^{(w)}$ denotes the actual spatial angular-acceleration bias term induced by the first-order motion state. The acceleration-level inverse mapping inherits the conditioning characteristics of $\mathbf{J}_{n,t}^{(w)}$ discussed above; hence, its sensitivity also increases as q_A approaches the singular boundary.

Accordingly, the six-dimensional task acceleration $\mathbf{A}_t^{(w)}$ referenced at the tool reference point can be written as

$$\mathbf{A}_t^{(w)} = \begin{pmatrix} \mathbf{a}_t^{(w)} \\ \boldsymbol{\alpha}_t^{(w)} \end{pmatrix} = \mathbf{L}_{v,t}^{(w)} \ddot{\mathbf{x}}_t^{(w)} + \mathbf{b}_{A,t}^{(w)} \tag{91}$$

$$\mathbf{b}_{A,t}^{(w)} = \begin{pmatrix} \mathbf{0}_{3\times 1} \\ \mathbf{b}_{\alpha,t}^{(w)} \end{pmatrix}, \boldsymbol{\alpha}_t^{(w)} = \begin{bmatrix} \alpha_{x,t}^{(w)} & \alpha_{y,t}^{(w)} & \alpha_{z,t}^{(w)} \end{bmatrix}^T$$

Differentiating the velocity-level relation in Equation (51) with respect to time gives

$$\mathbf{A}_t^{(w)} = \mathbf{L}_{v,t}^{(w)} \ddot{\mathbf{x}}_t^{(w)} + \dot{\mathbf{L}}_{v,t}^{(w)} \dot{\mathbf{x}}_t^{(w)} \tag{92}$$

A comparison of Equations (91) and (92) gives

$$\mathbf{b}_{A,t}^{(w)} = \dot{\mathbf{L}}_{v,t}^{(w)} \dot{\mathbf{x}}_t^{(w)} \tag{93}$$

Differentiating Equation (68) with respect to time yields

$$\mathbf{A}_t^{(w)} = \mathbf{T}_t^{(w)} \ddot{\mathbf{q}} + \dot{\mathbf{T}}_t^{(w)} \dot{\mathbf{q}} \tag{94}$$

where $\dot{\mathbf{T}}_t^{(w)}$ denotes the first-order time derivative of the unified allowable motion-screw matrix of the five-axis machine tool at the current position and velocity state. The first term on the right-hand side represents the linear acceleration contribution generated by the five-axis generalized acceleration through the current allowable motion-screw matrix, whereas the second term represents the velocity-quadratic coupling arising from the configuration-dependent variation of the allowable motion screws themselves. Rearranging Equation (94) gives

$$\mathbf{T}_t^{(w)} \ddot{\mathbf{q}} = \mathbf{A}_t^{(w)} - \dot{\mathbf{T}}_t^{(w)} \dot{\mathbf{q}} \tag{95}$$

Differentiating Equation (57) with respect to time gives

$$\dot{\mathbf{X}}_t^{(w)} = \begin{bmatrix} \mathbf{0}_{3\times 3} & -[\mathbf{v}_t^{(w)}\times] \\ \mathbf{0}_{3\times 3} & \mathbf{0}_{3\times 3} \end{bmatrix} \tag{96}$$

where $\dot{\mathbf{X}}_t^{(w)}$ denotes the first-order time derivative of the reference-point transformation matrix. Differentiating Equation (68) with respect to time gives

$$\dot{\mathbf{T}}_t^{(w)} = \dot{\mathbf{X}}_t^{(w)} \mathbf{J}_{s,t}^{(w)} + \mathbf{X}_t^{(w)} \dot{\mathbf{J}}_{s,t}^{(w)} \tag{97}$$

where $\dot{\mathbf{J}}_{s,t}^{(w)}$ denotes the first-order time derivative of the standard spatial screw Jacobian.

Differentiating Equation (64) with respect to time gives the time derivative of the spatial unit motion screw associated with the kth column as

$$\dot{\boldsymbol{\xi}}_{\theta,1}^{(w)} = 0, \quad \dot{\boldsymbol{\xi}}_{\theta,k}^{(w)} = \frac{d}{dt}\left(\mathrm{Ad}_{g^{(w)}} \boldsymbol{\Sigma}_k\right) = \mathrm{ad}_{\boldsymbol{\nu}^{(w)}}\left(\mathrm{Ad}_{g^{(w)}} \boldsymbol{\Sigma}_k\right) = \mathrm{ad}_{\boldsymbol{\nu}^{(w)}} \boldsymbol{\xi}_{\theta,k}^{(w)}, \quad k = 2, \ldots, 5 \tag{98}$$

$$\boldsymbol{\nu}_{k-1}^{(w)} = \left[\dot{\mathbf{g}}_{k-1}^{(w)} \mathbf{g}_{k-1}^{(w)}\right]^{\vee} = \sum_{i=1}^{k-1} \boldsymbol{\xi}_{\theta,i}^{(w)} \dot{\theta}_i$$

where $\dot{\boldsymbol{\xi}}_{\theta,k}^{(w)}$ denotes the first-order time derivative of the current spatial unit motion screw associated with the kth joint, and $\boldsymbol{\nu}_{k-1}^{(w)}$ denotes the cumulative spatial velocity screw generated by all preceding joints before the kth joint in the internal POE sequence. Furthermore, because ad is linear in its first argument,

$$\dot{\boldsymbol{\xi}}_{\theta,k}^{(w)} = \sum_{i=1}^{k-1} \dot{\boldsymbol{\theta}}_i \mathrm{ad}_{\boldsymbol{\xi}_{\theta,i}^{(w)}} \boldsymbol{\xi}_{\theta,k}^{(w)}, \quad k = 2, \ldots, 5 \tag{99}$$

which can be rearranged as

$$\dot{\boldsymbol{\xi}}_{\theta,1}^{(w)} = 0, \quad \dot{\boldsymbol{\xi}}_{\theta,k}^{(w)} = \sum_{i=1}^{k-1} \dot{\boldsymbol{\theta}}_i \left(\boldsymbol{\xi}_{\theta,i}^{(w)} \times \boldsymbol{\xi}_{\theta,k}^{(w)} \right), \quad k = 2, \ldots, 5 \tag{100}$$

According to the Lie-algebraic relation governing the time derivative of the adjoint-transformed screw coordinates and higher-order POE kinematics [11], the time derivative of the spatial unit motion screw in the kth column can be written in a unified form as

$$\dot{\boldsymbol{\xi}}_{\theta,k}^{(w)} = \mathrm{ad}_{\boldsymbol{\nu}_{k-1}^{(w)}} \boldsymbol{\xi}_{i_k,t}^{(w)} = \sum_{r=1}^{k-1} \dot{\boldsymbol{\theta}}_r \mathrm{ad}_{\boldsymbol{\xi}_{i_r,t}^{(w)}} \boldsymbol{\xi}_{i_k,t}^{(w)} \tag{101}$$

Assembling the derivatives of the five columns according to the internal POE sequence gives

$$\dot{\mathbf{J}}_{\theta,s,t}^{(w)} = [\dot{\boldsymbol{\xi}}_{\theta,1}^{(w)} \quad \dot{\boldsymbol{\xi}}_{\theta,2}^{(w)} \quad \dot{\boldsymbol{\xi}}_{\theta,3}^{(w)} \quad \dot{\boldsymbol{\xi}}_{\theta,4}^{(w)} \quad \dot{\boldsymbol{\xi}}_{\theta,5}^{(w)}] \tag{102}$$

where $\dot{\mathbf{J}}_{\theta,s,t}^{(w)}$ denotes the first-order time derivative of the standard spatial screw Jacobian arranged according to the internal POE sequence.

Since the permutation matrix $\mathbf{E}_q^{\theta}$ is constant, differentiating Equation (67) gives

$$\dot{\mathbf{J}}_{s,t}^{(w)} = \dot{\mathbf{J}}_{\theta,s,t}^{(w)} \mathbf{E}_q^{\theta} \tag{103}$$

Combining Equations (96), (97) and (103) yields the unified analytical expression formulated entirely in terms of the POE representation, adjoint transformations, and Lie brackets,

$$\dot{\mathbf{T}}_t^{(w)} = \dot{\mathbf{X}}_t^{(w)} \mathbf{J}_{s,t}^{(w)} + \mathbf{X}_t^{(w)} \dot{\mathbf{J}}_{\theta,s,t}^{(w)} \mathbf{E}_q^{\theta} \tag{104}$$

Premultiplying both sides of Equation (95) by $\mathbf{G}_t^{(w)}$ and rearranging gives the analytical inverse acceleration solution under the six-dimensional actual task acceleration,

$$\ddot{\mathbf{q}} = \mathbf{G}_t^{(w)} \left[\mathbf{A}_t^{(w)} - \dot{\mathbf{T}}_t^{(w)} \mathbf{G}_t^{(w)} \mathbf{L}_{v,t}^{(w)} \dot{\mathbf{x}}_t^{(w)} \right] \tag{105}$$

Substituting Equation (91) into Equation (105) then gives the final inverse acceleration solution under the unified machining-task input formulation,

$$\ddot{\mathbf{q}} = \mathbf{G}_t^{(w)} \left[\mathbf{L}_{v,t}^{(w)} \ddot{\mathbf{x}}_t^{(w)} + \mathbf{b}_{A,t}^{(w)} - \dot{\mathbf{T}}_t^{(w)} \mathbf{G}_t^{(w)} \mathbf{L}_{v,t}^{(w)} \dot{\mathbf{x}}_t^{(w)} \right] \tag{106}$$

The main emphasis of the proposed acceleration model is not to redefine the time-differentiation relation of the POE Jacobian but rather to retain the machining-task-variable-to-motion-screw mapping and the mechanism allowable-motion-screw mapping as two interconnected differential levels with distinct physical meanings. At the machining-task level, in $\mathbf{A}_t^{(w)} = \mathbf{L}_{v,t}^{(w)} \ddot{\mathbf{x}}_t^{(w)} + \dot{\mathbf{L}}_{v,t}^{(w)} \dot{\mathbf{x}}_t^{(w)}$, the term $\dot{\mathbf{L}}_{v,t}^{(w)} \dot{\mathbf{x}}_t^{(w)}$ represents the second-order geometric effects arising from the unit-sphere geometry of the tool-axis direction, the current orientation, and the time variation of the task-variable-to-motion-screw mapping.

At the mechanism-motion level, the term $\dot{\mathbf{T}}_t^{(w)}\dot{\mathbf{q}}$ in $\mathbf{A}_t^{(w)} = \mathbf{T}_t^{(w)}\ddot{\mathbf{q}} + \dot{\mathbf{T}}_t^{(w)}\dot{\mathbf{q}}$ represents the second-order motion coupling induced by the configuration-dependent variation of the allowable motion-screw basis of the machine tool.

In this way, the second-order geometric effects arising from the machining-task parameterization and the second-order motion coupling induced by the machine-tool topology are explicitly separated in both their mathematical expressions and physical origins, while the same actual task acceleration $\mathbf{A}_t^{(w)}$ provides a continuous interface between the two mapping levels. The computation of $\dot{\mathbf{T}}_t^{(w)}$ at the mechanism level continues to follow the established higher-order differential theory of the POE formulation, in which the time derivative of the spatial Jacobian and the Lie-algebra adjoint operator are used to generate the configuration-dependent variation terms of the individual allowable motion screws in a unified manner.

Consequently, this section establishes a first- and second-order continuous mapping framework of $\mathbb{R}^3 \times S^2 \to \mathfrak{se}(3) \to \mathbb{R}^5$, in which the position, velocity, and acceleration models are consistently derived from the same finite-pose model and the same set of mechanism screws. This treatment avoids conflating the second-order variation of the tool-axis direction with the actual spatial angular acceleration, while also preventing the second-order geometric terms in the task space from being mixed with the second-order configuration-dependent terms of the mechanism, thereby providing a unified state interface for the subsequent calculation of rigid-body accelerations of the physical components and the associated inertial loads.

4.3. Rigid-Body Dynamic Modeling

In this section, the rigid-body dynamic equations of the five-axis CNC machine tool are established based on the principle of virtual work. To facilitate motor selection, the following assumptions are adopted in the dynamic modeling:

(1) The contact friction forces between the components are neglected.

(2) All contacts between the components are assumed to form ideal kinematic pairs.

(3) The cutting spindle rotation about the tool axis is not introduced as an additional generalized coordinate. Consequently, the rotational kinetic energy, rotor-inertia contribution, and gyroscopic moment associated with the high-speed spindle rotation are not included in the present rigid-body validation.

(4) Motor-rotor inertia and transmission/reflected inertia associated with drive components are not included separately. The calculated generalized forces and torques therefore represent the mechanical-side loads associated with the modeled moving rigid bodies.

(5) No cutting force or cutting torque is applied in the numerical validation, i.e., $\mathbf{Q}_{\text{ext}} = \mathbf{0}$. External machining loads can subsequently be introduced through the wrench interface of the general dynamic formulation.

The inverse velocity and acceleration models describe the task motion of the tool relative to the workpiece, whereas rigid-body dynamics requires the physical motion of each actual moving rigid body relative to the fixed machine-bed coordinate frame. Therefore, the relative virtual screws used in the inverse velocity model cannot be directly employed as the motion screws of the physical bodies in the dynamic model. At the dynamics level, the formulation must return to the two actual physical kinematic chains of the machine tool, with $\mathbf{q}$, $\dot{\mathbf{q}}$, and $\ddot{\mathbf{q}}$ obtained from the inverse velocity and acceleration solutions serving as the unified inputs.

The generalized driving-force and driving-torque vector at the mechanical side of the five-axis machine tool is defined as

$$\mathbf{Q} = [F_X \quad F_Y \quad F_Z \quad M_A \quad M_C]^T \tag{107}$$

The rigid-body dynamic calculation is based on the physical motion of each actual rigid body relative to the fixed machine bed rather than on the tool–workpiece relative virtual chain. According to the machine-tool architecture, the ordered sets of actuated joints traversed by the moving rigid bodies are

$$\mathbf{A}_Y = \{Y\}, \quad \mathbf{A}_X = \{Y, X\}, \quad \mathbf{A}_Z = \mathcal{A}_t = \{Y, X, Z\}$$
$$\mathbf{A}_A = \{A\}, \quad \mathbf{A}_C = \{A, C\} \tag{108}$$

where $\mathbf{A}_i$ denotes the ordered set of actuated joints along the path from the fixed machine bed B_0 to the moving rigid body B_i. To consistently embed the local joint ordering of each subchain into the global XYZAC axis ordering, the following constant selection matrices are defined:

$$\boldsymbol{E}_Y = \begin{bmatrix} 0 & 1 & 0 & 0 & 0 \end{bmatrix}, \quad \boldsymbol{E}_A = \begin{bmatrix} 0 & 0 & 0 & 1 & 0 \end{bmatrix}$$
$$\boldsymbol{E}_x = \begin{bmatrix} 0 & 1 & 0 & 0 & 0 \\ 1 & 0 & 0 & 0 & 0 \end{bmatrix}, \quad \boldsymbol{E}_C = \begin{bmatrix} 0 & 0 & 0 & 1 & 0 \\ 0 & 0 & 0 & 0 & 1 \end{bmatrix}$$
$$\boldsymbol{E}_z = \boldsymbol{E}_t = \begin{bmatrix} 0 & 1 & 0 & 0 & 0 \\ 1 & 0 & 0 & 0 & 0 \\ 0 & 0 & 1 & 0 & 0 \end{bmatrix} \tag{109}$$

where $\mathbf{E}_i$ denotes the constant selection matrix that extracts the joint variables of the actual POE subchain associated with rigid body B_i from the global five-axis generalized coordinates. Accordingly, the local ordered joint-position, joint-velocity, and joint-acceleration vectors of the th rigid body are given by

$$\mathbf{q}_i = \mathbf{E}_i \mathbf{q}, \quad \dot{\mathbf{q}}_i = \mathbf{E}_i \dot{\mathbf{q}}, \quad \ddot{\mathbf{q}}_i = \mathbf{E}_i \ddot{\mathbf{q}} \tag{110}$$

where $\mathbf{q}_i$ denotes the local joint-position vector of the actual POE subchain associated with rigid body B_i, $\dot{\mathbf{q}}_i$ denotes the corresponding local joint-velocity vector, and $\ddot{\mathbf{q}}_i$ denotes the corresponding local joint-acceleration vector.

Suppose that the actual POE subchain of rigid body B_i contains n_i joints arranged in their physical order. Its pose relative to the machine-bed coordinate frame is given by

$$\mathbf{g}_i^{(0)} = \prod_{r=1}^{n_i} \mathrm{e}^{[\mathbf{S}_{i,r}^{(0)}]^{\wedge} \mathbf{q}_{i_r}} \mathbf{M}_i^{(0)} \tag{111}$$

where $\mathbf{g}_t^{(0)}$ denotes the current homogeneous pose of rigid body B_i relative to the machine-bed inertial coordinate frame, $\mathbf{S}_{i,r}^{(0)}$ denotes the zero-configuration unit motion screw of the rth joint in the subchain expressed in the machine-bed coordinate frame, $\mathbf{q}_{i_r}$ denotes the generalized displacement or rotation angle of the rth joint in the subchain, and $\mathbf{M}_i^{(0)}$ denotes the constant homogeneous transformation of rigid body B_i relative to the machine-bed coordinate frame when all actuated axes are at their zero configurations.

According to the spatial differential formulation of the POE representation, the spatial unit motion screw of the kth joint in the subchain of the ith rigid body at the current configuration is

$$\dot{\boldsymbol{\xi}}_{i,1}^{(0)} = \mathbf{S}_{i_1}^{(0)}, \quad \dot{\boldsymbol{\xi}}_{i,k}^{(0)} = \mathrm{Ad}_{\prod_{r=1}^{k-1} \mathrm{e}^{[\mathbf{S}_{i,r}^{(0)}]^{\wedge} \mathbf{q}_{i_r}}} \mathbf{S}_{i_k}^{(0)}, \quad k = 2, \ldots, n_i \tag{112}$$

where $\dot{\boldsymbol{\xi}}_{i,k}^{(0)}$ denotes the spatial unit motion screw of the kth joint in the actual POE subchain of rigid body B_i at the current configuration, expressed in the machine-bed coordinate frame. Assembling the columns according to the local POE ordering gives the local standard spatial Jacobian, which is then embedded into the unified five-axis generalized-coordinate space through the selection matrix:

$$\mathbf{J}_{s,i}^{(0)} = \begin{bmatrix} \boldsymbol{\xi}_{i,1}^{(0)} & \cdots & \boldsymbol{\xi}_{i,n_i}^{(0)} \end{bmatrix}, \quad \bar{\mathbf{J}}_{s,i}^{(0)} = \mathbf{J}_{s,i}^{(0)} \mathbf{E}_i \in \mathbb{R}^{6\times 5} \tag{113}$$

where $\mathbf{J}_{s,i}^{(0)}$ denotes the standard spatial screw Jacobian of the local POE subchain associated with rigid body B_i, and $\bar{\mathbf{J}}_{s,i}^{(0)}$ denotes the 6×5 standard spatial Jacobian embedded according to the global XYZAC axis ordering.

Let O_i be the selected body-fixed reference point of rigid body B_i, whose current position vector in the machine-bed coordinate frame is $\mathbf{p}_{O_i}^{(0)}$. The reference-point transformation matrix that maps the standard spatial motion screw to a parameterization whose first three components are the actual linear velocity of point O_i is defined as

$$\mathbf{X}_i^{(0)} = \begin{bmatrix} \mathbf{I}_3 & -[\mathbf{p}_{O_i}^{(0)}\times] \\ \mathbf{0}_{3\times 3} & \mathbf{I}_3 \end{bmatrix} \tag{114}$$

where $\mathbf{X}_i^{(0)}$ denotes the 6×6 reference-point transformation matrix that converts the standard spatial motion screw into a representation whose first three components correspond to the actual linear velocity of the rigid-body reference point O_i. Accordingly, the unified five-axis motion-screw matrix of the ith rigid body referenced at O_i is

$$\mathbf{T}_i^{(0)} = \mathbf{X}_i^{(0)} \bar{\mathbf{J}}_{s,i}^{(0)} \in \mathbb{R}^{6\times 5} \tag{115}$$

where $\mathbf{T}_i^{(0)}$ denotes the unified motion-screw matrix of rigid body B_i at reference point O_i, arranged according to the global five-axis ordering.

The six-dimensional physical velocity and acceleration vectors of rigid body B_i at reference point O_i are, respectively,

$$\boldsymbol{v}_i^{(0)} = \begin{pmatrix} \mathbf{v}_{O_i}^{(0)} \\ \boldsymbol{\omega}_i^{(0)} \end{pmatrix} = \mathbf{T}_i^{(0)} \dot{\mathbf{q}}, \mathbf{A}_i^{(0)} = \begin{pmatrix} \mathbf{a}_{O_i}^{(0)} \\ \boldsymbol{\alpha}_i^{(0)} \end{pmatrix} = \mathbf{T}_i^{(0)} \ddot{\mathbf{q}} + \dot{\mathbf{T}}_i^{(0)} \dot{\mathbf{q}} \tag{116}$$

where $\boldsymbol{v}_i^{(0)}$ denotes the six-dimensional physical velocity vector of rigid body $\boldsymbol{v}_i^{(0)}$ at reference point O_i expressed in the machine-bed coordinate frame, $\mathbf{v}_{O_i}^{(0)}$ denotes the actual linear velocity of reference point $\boldsymbol{\omega}_i^{(0)}$ denotes the actual spatial angular-velocity vector of rigid body B_i, $\mathbf{A}_i^{(0)}$ denotes the six-dimensional physical acceleration vector of rigid body B_i at reference point $\mathbf{a}_{O_i}^{(0)}$ denotes the actual linear acceleration of reference point O_i, $\boldsymbol{\alpha}_i^{(0)}$ denotes the actual spatial angular-acceleration vector of rigid body B_i, and $\dot{\mathbf{T}}_i^{(0)}$ denotes the first-order time derivative of the unified motion-screw matrix of rigid body B_i. As in the inverse acceleration model, the general expression for $\dot{\mathbf{T}}_i^{(0)}$ is

$$\dot{\mathbf{T}}_i^{(0)} = \dot{\mathbf{X}}_i^{(0)} \bar{\mathbf{J}}_{s,i}^{(0)} + \mathbf{X}_i^{(0)} \dot{\bar{\mathbf{J}}}_{s,i}^{(0)} \tag{117}$$

$$\dot{\mathbf{X}}_i^{(0)} = \begin{bmatrix} \mathbf{0}_{3\times 3} & -[\mathbf{v}_{O_i}^{(0)}\times] \\ \mathbf{0}_{3\times 3} & \mathbf{0}_{3\times 3} \end{bmatrix}$$

where $\dot{\mathbf{X}}_i^{(0)}$ denotes the first-order time derivative of the reference-point transformation matrix of rigid body B_i, and $\dot{\mathbf{J}}_{s,i}^{(0)}$ denotes the time derivative of the standard spatial Jacobian embedded in the global axis ordering. The time derivative of each Jacobian column is obtained in a unified manner using the same Lie-bracket relation as that employed in the inverse acceleration model,

$$\boldsymbol{\xi}_{i,1}^{(0)} = 0, \quad \boldsymbol{\xi}_{i,k}^{(0)} = \sum_{r=1}^{k-1} \dot{\mathbf{q}}_{i_r} \mathrm{ad}_{\boldsymbol{\xi}_{i,r}^{(0)}} \boldsymbol{\xi}_{i,k}^{(0)}, \quad k = 2, \ldots, n_i \tag{118}$$

where $\dot{\boldsymbol{\xi}}_{i,k}^{(0)}$ denotes the first-order time derivative of the current spatial unit motion screw associated with the kth joint in the subchain of rigid body B_i.

The mass properties of each rigid body are generally specified in its own body-fixed coordinate frame. Let the mass of rigid body B_i be m_i, the position vector from the body reference point O_i to the center of mass G_i be $\mathbf{r}_{G_i/O_i}^{(0)}$, and the inertia tensor about the center of mass be $\mathbf{I}_{G_i}^{(0)}$. Extracting the rotation matrix $\mathbf{R}_i^{(0)}$ from the current pose, the center-of-mass offset and the inertia tensor about the center of mass expressed in the machine-bed inertial coordinate frame are, respectively,

$$\mathbf{r}_{G_i/O_i}^{(0)} = \mathbf{R}_i^{(0)} \mathbf{r}_{G_i/O_i}^{(i)}, \quad \mathbf{I}_{G_i}^{(0)} = \mathbf{R}_i^{(0)} \mathbf{I}_{G_i}^{(i)} \left(\mathbf{R}_i^{(0)}\right)^T \tag{119}$$

where $\mathbf{r}_{G_i/O_i}^{(0)}$ denotes the position vector from the rigid-body reference point O_i to the center of mass G_i expressed in the machine-bed coordinate frame, $\mathbf{R}_i^{(0)}$ denotes the current rotation matrix of the body-fixed coordinate frame of rigid body B_i relative to the machine-bed coordinate frame, $\mathbf{r}_{G_i/O_i}^{(i)}$ denotes the position vector of the center of mass relative to reference point O_i expressed in the body-fixed coordinate frame, $\mathbf{I}_{G_i}^{(0)}$ denotes the inertia tensor of rigid body B_i about its center of mass expressed in the machine-bed coordinate frame, and $\mathbf{I}_{G_i}^{(i)}$ denotes the corresponding inertia tensor expressed in the body-fixed coordinate frame.

For the same rigid body, the rigid-body velocity and acceleration relationships between reference point O_i and center of mass G_i are, respectively,

$$\begin{aligned} \mathbf{v}_{G_i}^{(0)} &= \mathbf{v}_{O_i}^{(0)} + \boldsymbol{\omega}_i^{(0)} \times \mathbf{r}_{G_i/O_i}^{(0)} = \mathbf{v}_{O_i}^{(0)} - \left[\mathbf{r}_{G_i/O_i}^{(0)} \times\right] \boldsymbol{\omega}_i^{(0)} \\ \mathbf{a}_{G_i}^{(0)} &= \mathbf{a}_{O_i}^{(0)} + \boldsymbol{\alpha}_i^{(0)} \times \mathbf{r}_{G_i/O_i}^{(0)} + \boldsymbol{\omega}_i^{(0)} \times \left(\boldsymbol{\omega}_i^{(0)} \times \mathbf{r}_{G_i/O_i}^{(0)}\right) \end{aligned} \tag{120}$$

where $\mathbf{v}_{G_i}^{(0)}$ denotes the actual linear velocity of the center of mass G_i of rigid body B_i expressed in the machine-bed coordinate frame, and $\mathbf{a}_{G_i}^{(0)}$ denotes the actual linear acceleration of the rigid-body center of mass expressed in the machine-bed coordinate frame.

The kinetic energy of rigid body B_i is

$$T_i = \frac{1}{2} m_i \left(\mathbf{v}_{G_i}^{(0)}\right)^T \mathbf{v}_{G_i}^{(0)} + \frac{1}{2} \left(\boldsymbol{\omega}_i^{(0)}\right)^T \mathbf{I}_{G_i}^{(0)} \boldsymbol{\omega}_i^{(0)} \tag{121}$$

where T_i denotes the instantaneous kinetic energy of the rigid body, and T_i denotes its mass. With Equation (120) being substituted into Equation (121) and rearranging in terms of the six-dimensional reference-point velocity $\boldsymbol{v}_i^{(0)}$, the kinetic energy can be written in the unified quadratic form

$$T_i = \frac{1}{2} \left(\boldsymbol{v}_i^{(0)}\right)^T \mathbf{M}_i^{(0)} \boldsymbol{v}_i^{(0)} \tag{122}$$

$$\mathbf{M}_i^{(0)} = \begin{bmatrix} m_i\mathbf{I}_3 & -m_i\left[\mathbf{r}_{G_i/O_i}^{(0)}\times\right] \\ m_i\left[\mathbf{r}_{G_i/O_i}^{(0)}\times\right] & \mathbf{I}_{G_i}^{(0)} - m_i\left[\mathbf{r}_{G_i/O_i}^{(0)}\times\right]^2 \end{bmatrix}$$

where $\mathbf{M}_i^{(0)}$ denotes the reference-point inertia matrix of rigid body B_i expressed in the machine-bed coordinate frame, with moments taken about the reference point O_i.

According to the parallel-axis theorem, the three-dimensional inertia tensor of the rigid body about the reference point O_i is defined as

$$\mathbf{I}_{O_i}^{(0)} = \mathbf{I}_{G_i}^{(0)} - m_i\left[\mathbf{r}_{G_i/O_i}^{(0)}\times\right]^2 \tag{123}$$

where $\mathbf{I}_{O_i}^{(0)}$ denotes the 3×3 rotational inertia tensor of the rigid body about the reference point O_i, expressed in the machine-bed coordinate frame.

In the machine-bed inertial coordinate frame, the inertial force corresponding to the Newton translational equation of the center of mass of the ith rigid body is

$$\mathbf{f}_i^{I,(0)} = m_i\mathbf{a}_{G_i}^{(0)} \tag{124}$$

where $\mathbf{f}_i^{I,(0)}$ denotes the resultant inertial force required to produce the prescribed center-of-mass acceleration, expressed in the machine-bed coordinate frame.

The Euler rotational equation of the rigid body about its center of mass is

$$\boldsymbol{\tau}_{G_i}^{I,(0)} = \mathbf{I}_{G_i}^{(0)}\boldsymbol{\alpha}_i^{(0)} + \boldsymbol{\omega}_i^{(0)}\times\left(\mathbf{I}_{G_i}^{(0)}\boldsymbol{\omega}_i^{(0)}\right) \tag{125}$$

where $\boldsymbol{\tau}_{G_i}^{I,(0)}$ denotes the inertial moment of rigid body B_i about its center of mass, G_i.

Transferring the inertial moment from the center of mass to the reference point O_i gives

$$\boldsymbol{\tau}_{O_i}^{I,(0)} = \boldsymbol{\tau}_{G_i}^{I,(0)} + \mathbf{r}_{G_i/O_i}^{(0)}\times\mathbf{f}_i^{I,(0)} \tag{126}$$

where $\boldsymbol{\tau}_{O_i}^{I,(0)}$ denotes the inertial moment of rigid body B_i about the reference point O_i.

Combining the resultant inertial force and the inertial moment about O_i defines the six-dimensional Newton–Euler inertial wrench screw as

$$\mathbf{F}_i^{I,(0)} = \begin{pmatrix} \mathbf{f}_i^{I,(0)} \\ \boldsymbol{\tau}_{O_i}^{I,(0)} \end{pmatrix} \tag{127}$$

where $\mathbf{F}_i^{I,(0)}$ denotes the six-dimensional Newton–Euler inertial wrench screw of rigid body B_i about the reference point O_i.

Rearranging Equations (119)–(127) into a unified six-dimensional form gives

$$\mathbf{F}_i^{I,(0)} = \mathbf{M}_i^{(0)}\mathbf{A}_i^{(0)} + \mathbf{c}_i^{I,(0)} \tag{128}$$

$$\mathbf{c}_i^{I,(0)} = \begin{bmatrix} m_i\boldsymbol{\omega}_i^{(0)}\times\left(\boldsymbol{\omega}_i^{(0)}\times\mathbf{r}_{G_i/O_i}^{(0)}\right) \\ m_i\mathbf{r}_{G_i/O_i}^{(0)}\times\left[\boldsymbol{\omega}_i^{(0)}\times\left(\boldsymbol{\omega}_i^{(0)}\times\mathbf{r}_{G_i/O_i}^{(0)}\right)\right] + \boldsymbol{\omega}_i^{(0)}\times\left(\mathbf{I}_{G_i}^{(0)}\boldsymbol{\omega}_i^{(0)}\right) \end{bmatrix}$$

where $\mathbf{c}_i^{I,(0)}$ denotes the six-dimensional velocity-quadratic inertial term induced by the angular velocity. Its upper three components correspond to the inertial force associated with the centripetal acceleration caused by the center-of-mass offset, whereas its lower three components correspond to the gyroscopic moment expressed about the reference point. This expression is fully equivalent to the classical Newton–Euler equations while remaining

compatible with the six-dimensional motion-screw representation and the subsequent virtual-work projection.

When the Z_0 axis of the machine-bed coordinate frame is defined as vertically upward, the gravitational acceleration vector $\mathbf{g}^{(0)}$ is

$$\mathbf{g}^{(0)} = \begin{pmatrix} 0 & 0 & -g \end{pmatrix}^T \tag{129}$$

Accordingly, the gravitational wrench screw of rigid body B_i about the reference point O_i is written as

$$\mathbf{F}_i^{g,(0)} = \begin{bmatrix} m_i \mathbf{g}^{(0)} \\ \mathbf{r}_{G_i/O_i}^{(0)} \times m_i \mathbf{g}^{(0)} \end{bmatrix} \tag{130}$$

where $\mathbf{F}_i^{g,(0)}$ denotes the six-dimensional gravitational wrench screw of rigid body B_i about the reference point O_i.

If an external cutting force, clamping force, or other applied load is initially given in wrench-screw form in the workpiece coordinate frame of the rotary table,

$$\mathbf{F}_{i,a}^{ext} = \begin{bmatrix} \mathbf{f}_{i,a}^{ext} \\ \boldsymbol{\tau}_{i,a}^{ext} \end{bmatrix} \tag{131}$$

where $\mathbf{F}_{i,a}^{ext}$ denotes the external six-dimensional wrench screw acting on rigid body B_i, expressed in coordinate frame $\mathcal{K}_a$ about its selected moment reference point, $\mathbf{f}_{i,a}^{ext}$ denotes the resultant external force, and $\boldsymbol{\tau}_{i,a}^{ext}$ denotes the resultant external moment. Using the power duality between motion and wrench screws, the external wrench can be transformed consistently to the machine-bed coordinate frame $\mathcal{K}_0$ and reference point O_i through the dual adjoint transformation,

$$\mathbf{F}_i^{ext,(0)} = \mathrm{Ad}_{\mathbf{g}_{0\leftarrow a,i}}^{-T} \mathbf{F}_{i,a}^{ext} \tag{132}$$

where $\mathbf{F}_i^{ext,(0)}$ denotes the external wrench screw expressed in the machine-bed coordinate frame and referenced at O_i, and $\mathbf{g}_{0\leftarrow a,i}$ denotes the homogeneous transformation from the original coordinate frame/reference point of the applied load to the machine-bed coordinate frame/reference point O_i. To realize the prescribed motion, the resultant wrench that must be balanced by the actuation system is defined as

$$\mathbf{F}_i^{req,(0)} = \mathbf{F}_i^{I,(0)} - \mathbf{F}_i^{g,(0)} - \mathbf{F}_i^{ext,(0)} \tag{133}$$

where $\mathbf{F}_i^{req,(0)}$ denotes the six-dimensional required wrench that must be balanced by the actuation system to realize the prescribed motion of rigid body B_i.

Based on the power duality between motion screws and wrench screws and the principle of virtual work [15,16], the generalized driving forces can be obtained by projecting the required rigid-body wrenches onto the admissible generalized motions. For any admissible five-axis virtual velocity $\delta\dot{\mathbf{q}}$, the virtual velocity screw at the reference point of rigid body B_i is

$$\delta \boldsymbol{v}_i^{(0)} = \mathbf{T}_i^{(0)} \delta\dot{\mathbf{q}} \tag{134}$$

where $\delta \boldsymbol{v}_i^{(0)}$ denotes the virtual velocity screw at the reference point of rigid body B_i induced by an arbitrary admissible five-axis virtual velocity.

The virtual power exerted by the generalized driving forces and torques at the mechanical axes is $\mathbf{Q}^T \delta\dot{\mathbf{q}}$, while the total virtual power associated with the required wrench screws of all rigid bodies is obtained by summing their individual contributions. Neglecting the virtual power of the ideal constraint wrench screws gives

$$\mathbf{Q}^T \delta\dot{\mathbf{q}} - \sum_{i\in\mathcal{B}_m} \left(\mathbf{F}_i^{req,(0)}\right)^T \delta \boldsymbol{v}_i^{(0)} = 0 \tag{135}$$

where $\mathcal{B}_m$ denotes the set of moving rigid bodies included in the summation of the actuated-axis dynamics. Substituting Equation (134) into Equation (135) gives

$$\left[\mathbf{Q} - \sum_{i\in\mathcal{B}_m} \left(\mathbf{T}_i^{(0)}\right)^T \mathbf{F}_i^{req,(0)}\right]^T \delta\dot{\mathbf{q}} = 0 \tag{136}$$

Since the above relation must hold for arbitrary $\delta\dot{\mathbf{q}}$, the vector in parentheses must be $\mathbf{0}$, yielding the fundamental screw-based expression for the rigid-body inverse dynamics of the complete machine tool:

$$\mathbf{Q} = \sum_{i\in\mathcal{B}_m} \left(\mathbf{T}_i^{(0)}\right)^T \mathbf{F}_i^{req,(0)} \tag{137}$$

Substituting the inertial, gravitational, and external-load terms into Equation (137) gives the complete directly computable form

$$\mathbf{Q} = \sum_{i\in\mathcal{B}_m} \left(\mathbf{T}_i^{(0)}\right)^T \left\{\mathbf{M}_i^{(0)}\left[\mathbf{T}_i^{(0)}\ddot{\mathbf{q}} + \dot{\mathbf{T}}_i^{(0)}\dot{\mathbf{q}}\right] + \mathbf{c}_i^{I,(0)} - \mathbf{F}_i^{g,(0)} - \mathbf{F}_i^{ext,(0)}\right\} \tag{138}$$

Equation (138) constitutes the core inverse-dynamics equation of this section. All of its inputs can be obtained from the kinematic states, the actual physical POE subchains, and the mass properties introduced above. The five actuated axes X, Y, Z, A, and C are thereby solved in a unified manner using the same five-dimensional generalized coordinates and the same motion-screw/wrench-screw dual projection framework.

To reveal the correspondence between Equation (138) and the classical multibody dynamic equations, all terms linearly associated with $\ddot{\mathbf{q}}$ are collected to define the five-axis joint-space inertia matrix $\mathbf{D}(\mathbf{q})$ as

$$\mathbf{D}(\mathbf{q}) = \sum_{i\in\mathcal{B}_m} \left(\mathbf{T}_i^{(0)}\right)^T \mathbf{M}_i^{(0)} \mathbf{T}_i^{(0)} \in \mathbb{R}^{5\times 5} \tag{139}$$

All velocity-dependent terms arising from the configuration-dependent variation of the motion-screw matrices and from the angular velocities of the rigid bodies are then collected to define

$$\mathbf{H}(\mathbf{q},\dot{\mathbf{q}}) = \sum_{i\in B_m} \left(\mathbf{T}_i^{(0)}\right)^T \left[\mathbf{M}_i^{(0)}\dot{\mathbf{T}}_i^{(0)}\dot{\mathbf{q}} + \mathbf{c}_i^{I,(0)}\right] \tag{140}$$

where $\mathbf{H}(\mathbf{q},\dot{\mathbf{q}})$ denotes the five-dimensional velocity-coupling generalized force comprising the contributions from variations of the Jacobian/motion-screw matrices, centripetal terms, and gyroscopic terms.

The gravitational generalized-force vector is defined as

$$\mathbf{G}_g(\mathbf{q}) = -\sum_{i\in\mathcal{B}_m} \left(\mathbf{T}_i^{(0)}\right)^T \mathbf{F}_i^{g,(0)} \tag{141}$$

where $\mathbf{G}_g(\mathbf{q})$ denotes the five-dimensional gravitational generalized-force vector obtained by projecting the gravitational wrenches of all moving rigid bodies through the principle of virtual work.

The generalized external load obtained by mapping the environmental external loads into the five-axis generalized-coordinate space is defined as

$$\mathbf{Q}_{ext}(\mathbf{q}) = \sum_{i \in \mathcal{B}_m} \left(\mathbf{T}_i^{(0)}\right)^T \mathbf{F}_i^{ext,(0)} \tag{142}$$

where $\mathbf{Q}_{ext}(\mathbf{q})$ denotes the generalized external-load vector obtained by projecting all environmental external loads into the five-axis generalized-coordinate space.

Accordingly, Equation (138) can be written in the standard joint-space form

$$\mathbf{Q} = \mathbf{D}(\mathbf{q})\ddot{\mathbf{q}} + \mathbf{H}(\mathbf{q}, \dot{\mathbf{q}}) + \mathbf{G}_g(\mathbf{q}) - \mathbf{Q}_{ext}(\mathbf{q}) \tag{143}$$

Because each $\mathbf{M}_i^{(0)}$ is constructed from a positive mass and a positive-definite rotational inertia tensor, and because the moving rigid bodies provide sufficient inertial contributions to the five generalized degrees of freedom at nonsingular configurations, $\mathbf{D}(\mathbf{q})$ is symmetric, i.e.,

$$\mathbf{D}(\mathbf{q})^T = \mathbf{D}(\mathbf{q}) \tag{144}$$

Meanwhile, the power consistency resulting from the virtual-work projection can serve as an important numerical check for the dynamic implementation,

$$\mathbf{Q}^T\dot{\mathbf{q}} = \sum_{i \in \mathcal{B}_m} \left(\mathbf{F}_i^{req,(0)}\right)^T \boldsymbol{v}_i^{(0)} \tag{145}$$

At the dynamics level, this section establishes a hierarchical screw-based modeling framework that is consistently interfaced with the preceding task-space differential kinematics. The tool–workpiece relative motion is described using a relative virtual screw chain, whose primary role is to establish a compact mapping between the machining task and the five-axis generalized states. In contrast, the computation of mass, inertia, gravity, and external loads must return to the actual physical POE subchains of the moving rigid bodies relative to the fixed machine bed. The two types of kinematic chains are connected through the unified generalized states $\mathbf{q}$, $\dot{\mathbf{q}}$, and $\ddot{\mathbf{q}}$, thereby ensuring that the relative virtual motion used for machining-task representation is not directly employed in Newton–Euler inertia calculations involving physical mass properties.

On this basis, the actual spatial velocity, spatial acceleration, and Newton–Euler required wrench screw of each moving rigid body are all represented in a unified six-dimensional screw form and projected into the five-axis generalized-coordinate space through the power duality between motion screws and wrench screws. Consequently, the generalized states obtained from the preceding task-space differential kinematics can be transferred continuously to the rigid-body inverse dynamics of the physical components, while external loads can likewise be incorporated consistently into the dynamic equations through wrench screws and dual adjoint transformations. This hierarchical modeling architecture primarily resolves the interface-consistency problem between relative task-motion descriptions and physical inertia calculations of the actual rigid bodies while providing a unified rigid-body motion basis and external-wrench interface for subsequent extensions to structural elastodynamics, joint/interface flexibility, and machining-load modeling.

4.4. Validation of the Rigid-Body Dynamic Model

Given the geometric and inertial parameters of the rigid-body dynamic model, as listed in Tables 4 and 5 , respectively, and prescribed tool machining-task variables together with their first- and second-order motion variables in the machining-task space, the proposed model is used to calculate the generalized driving-force and driving-torque profiles at the mechanical side of the five-axis machine tool. The analytical results are then compared with the software simulation results obtained under the same conditions to validate the proposed rigid-body dynamic model.

Table 4. Scale parameters (mm).

l_{x_1}	l_{y_1}	l_{y_2}	l_{y_3}	l_{z_1}	l_{z_2}	l_{z_3}	l_{z_4}
0	440	222	218	1085	−59	768	141

Table 5. Inertia and mass parameters.

Inertia	Value (kg · mm^2)	Mass	Value (kg)
$\mathbf{I}_0$	$\begin{bmatrix} 232741732.698 & 565961.438 & 58662.551 \\ 565961.438 & 238170728.759 & -32720692.282 \\ 58662.551 & -32720692.282 & 283595684.666 \end{bmatrix}$	m_0	482.389
$\mathbf{I}_y$	$\begin{bmatrix} 6696179.042 & 429902.451 & 157230.768 \\ 429902.451 & 17423195.191 & 1029229.707 \\ 157230.768 & 1029229.707 & 17752544.682 \end{bmatrix}$	m_y	98.558
$\mathbf{I}_x$	$\begin{bmatrix} 2927691.214 & 13574.469 & 13892.359 \\ 13574.469 & 3113921.314 & 120754.978 \\ 13892.359 & 120754.978 & 501751.004 \end{bmatrix}$	m_x	27.714
$\mathbf{I}_z$	$\begin{bmatrix} 7783244.427 & 159.113 & -1339.942 \\ 159.113 & 7877922.277 & -114182.381 \\ -1339.942 & -114182.381 & 962341.125 \end{bmatrix}$	m_z	57.411
$\mathbf{I}_t$	$\begin{bmatrix} 288.704 & 0 & 0 \\ 0 & 256.147 & 4.550 \\ 0 & 4.550 & 112.943 \end{bmatrix}$	m_t	0.202
$\mathbf{I}_a$	$\begin{bmatrix} 541468.825 & -3345.902 & 178473.522 \\ -3345.902 & 6652446.338 & -653.787 \\ 178473.522 & -653.787 & 6632098.707 \end{bmatrix}$	m_a	40.362
$\mathbf{I}_c$	$\begin{bmatrix} 151085.092 & 107.809 & 218.235 \\ 107.809 & 151044.746 & -41.278 \\ 218.235 & -41.278 & 124651.042 \end{bmatrix}$	m_c	12.431

Note: Bold symbols denote the inertia tensors (3 × 3 matrices), whereas non-bold italic symbols denote the corresponding scalar masses.

The preceding formulation is written for a general body reference point O_i, which does not necessarily coincide with the center of mass. In the numerical model used for the present validation, however, the body-fixed dynamic coordinate frame of each moving component is redefined with its origin at the corresponding center of mass G_i. Therefore, $\mathbf{r}^{(i)}_{G_i/O_i} = \mathbf{0}$ for all moving rigid bodies considered in the validation. The inertia tensors reported in Table 5 are evaluated about these body-frame origins, which coincide with the respective centers of mass, and are expressed in the corresponding body-fixed coordinate axes.

The comparison simulation was performed using SOLIDWORKS 2022 Motion Analysis. The same prescribed motion histories were applied to the analytical and simulation models, and the generalized reaction forces/torques were calculated independently by the SOLIDWORKS Motion solver without importing any analytical force/torque predictions. The comparison results were sampled at an interval of 0.04 s. All remaining solver and convergence settings were retained at the SOLIDWORKS Motion 2022 default values, with no user-defined tolerance settings imposed. The SOLIDWORKS comparison model was constructed from the three-dimensional assembly, mass/inertia properties, and joint constraints independently of the analytical inverse-dynamics equations. The same prescribed motion histories were used as common inputs, whereas the reaction forces and torques were calculated internally by SOLIDWORKS Motion without importing the analytical force/torque results.

All analytical dynamic calculations were performed internally in SI units: dimensions and inertia tensors reported in mm and kg·mm^2 were converted to m and kg·m^2, respectively, while forces and torques were evaluated in N and N·m; N·mm was used only when reporting rotary-axis torque results for readability.

To quantitatively evaluate the agreement between the analytical rigid-body dynamic model and the simulation, the prediction error of the j-th mechanical axis is defined as

$$e_{Q,j}(k) = Q_{j,\text{model}}(k) - Q_{j,\text{sim}}(k), \quad j \in \{X, Y, Z, A, C\} \tag{146}$$

where $Q_{j,\text{model}}$ denotes the generalized driving force or torque predicted by the proposed rigid-body dynamic model, and $Q_{j,\text{sim}}$ denotes the corresponding simulation result. The RMSE and maximum absolute error are calculated as

$$\text{RMSE}_{Q,j} = \sqrt{\frac{1}{N}\sum_{k=1}^{N} e_{Q,j}^2(k)}, E_{Q,j}^{\max} = \max_{1 \le k \le N} |e_{Q,j}(k)| \tag{147}$$

Figure 3 presents the time-domain comparisons of the generalized driving forces and torques predicted by the analytical model and obtained from the simulation.

The quantitative comparison results are summarized in Table 6. For the X-, Y-, and Z-axis driving forces, the RMSE values are 0.0305911, 0.0821185, and 0.0116695 N, respectively, while the corresponding maximum absolute errors are 0.197856, 0.531176, and 0.0756092 N. For the A- and C-axis driving torques, the RMSE values are 1.39897 and 0.59229 N·mm, with maximum absolute errors of 8.76912 and 3.70414 N·mm, respectively. The quantitative error metrics, together with the time-domain comparisons in Figure 3, demonstrate that the proposed rigid-body inverse-dynamics model reproduces the generalized mechanical driving-force and driving-torque responses of the simulation with good consistency under the investigated machining trajectory. The coefficients of determination for the five axes are 0.999703, 0.999703, 0.999702, 0.999992 and 0.999671, further confirming the consistency of the predicted response trends and amplitudes.

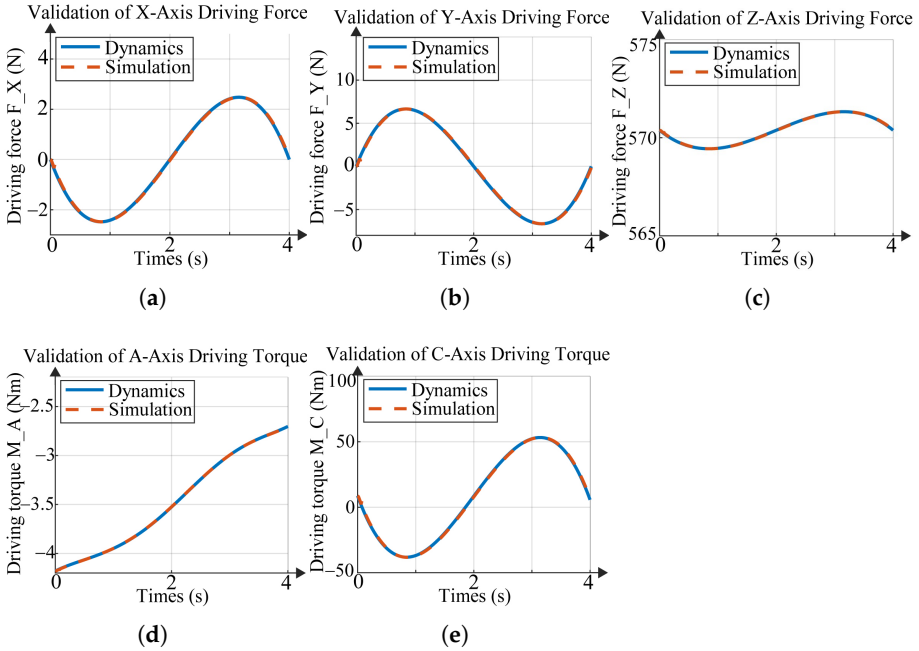

Figure 3. Validation of the generalized driving forces and driving torques at the mechanical side: (**a**) X-axis. (**b**) Y-axis. (**c**) Z-axis. (**d**) A-axis. (**e**) C-axis..

Table 6. Error metrics for the predicted force and torque components.

Axis	RMSE	Standard Deviation	Maximum Absolute Error	R^2
X	0.0305911 N	0.0306268 N	0.197856 N	0.999703
Y	0.0821185 N	0.0822141 N	0.531176 N	0.999703
Z	0.0116695 N	0.0116715 N	0.0756092 N	0.999702
A	1.39897 N·mm	1.38916 N·mm	8.76912 N·mm	0.999992
C	0.59229 N·mm	0.592808 N·mm	3.70414 N·mm	0.999671

The physical characteristics of the force/torque profiles can be interpreted from the joint-space form of the rigid-body dynamics, $\mathbf{Q} = \mathbf{D}(\mathbf{q})\ddot{\mathbf{q}} + \mathbf{H}(\mathbf{q}, \dot{\mathbf{q}}) + \mathbf{G}_g(\mathbf{q})$, because no external cutting load is applied in the present validation. The variations of the X- and Y-axis driving forces are mainly associated with the translational inertial response generated by the prescribed axis accelerations, together with the configuration-dependent coupling terms. For the vertical Z-axis, the gravitational contribution of the vertically supported moving masses produces an additional load component superimposed on the acceleration-dependent variation. The A- and C-axis torque profiles are primarily associated with the rotational inertias of the rotary-side components and their configuration-dependent inertial coupling. The velocity-dependent term $\mathbf{H}(\mathbf{q}, \dot{\mathbf{q}})$, including Jacobian-variation, centripetal, and gyroscopic contributions, becomes more pronounced during portions of the trajectory with larger generalized velocities. Therefore, the profiles in Figure 3 reflect the combined effects of inertial acceleration, gravity, and velocity-dependent rigid-body coupling rather than externally applied machining loads.

To further distinguish the two second-order effects introduced in Section 4.2, the generalized acceleration is decomposed into

$$\ddot{\mathbf{q}} = \ddot{\mathbf{q}}_{\text{dir}} + \ddot{\mathbf{q}}_{\text{geo}} + \ddot{\mathbf{q}}_{\text{cfg}} \tag{148}$$

where

$$\ddot{\mathbf{q}}_{\text{geo}} = \mathbf{G}_t^{(w)} \dot{\mathbf{L}}_{v,t}^{(w)} \dot{\mathbf{x}}_t^{(w)} \tag{149}$$

represents the task-geometry-induced second-order contribution, whereas

$$\ddot{\mathbf{q}}_{\text{cfg}} = -\mathbf{G}_t^{(w)} \dot{\mathbf{T}}_t^{(w)} \dot{\mathbf{q}} \tag{150}$$

represents the mechanism-configuration-induced contribution. Their RMS and maximum absolute values over the validation trajectory are summarized in Table 7. This decomposition quantifies the separate effects of the two terms without altering the original prescribed trajectory or dynamic model.

Table 7. Acceleration-level consistency evaluation.

Axis	RMS of $\ddot{q}_{\text{geo}}$	Max. $\lvert\ddot{q}_{\text{geo}}\rvert$	RMS of $\ddot{q}_{\text{cfg}}$	Max. $\lvert\ddot{q}_{\text{cfg}}\rvert$
X	24.30855 mm/s^2	45.46860 mm/s^2	52.83503 mm/s^2	97.48313 mm/s^2
Y	23.15095 mm/s^2	42.50388 mm/s^2	4.335554 mm/s^2	9.147783 mm/s^2
Z	2.808974 mm/s^2	6.041289 mm/s^2	28.26989 mm/s^2	52.89073 mm/s^2
A	3.704957 deg/s^2	6.878589 deg/s^2	1.031518×10^{-16} deg/s^2	5.963540×10^{-16} deg/s^2
C	5.930068 deg/s^2	10.98543 deg/s^2	0	0

The purpose of the present dynamic validation also differs from the flexible multibody studies in Refs. [17–19]. Huynh and Altintas [17] developed a position-dependent flexible multibody model including structural modes and joint/interface flexibility; Ref. [18] further coupled tool-path commands, inverse kinematics, servo control, and structural vibration,

while Bilgili et al. [19] focused on improving the computational efficiency of reduced-order multibody dynamics. In contrast, the present model intentionally retains the rigid-body level and validates the analytical transmission from machining-task motion to the generalized driving forces and torques. Its advantage is therefore not a higher structural-dynamic fidelity than Refs. [17–19], but an explicit and physically traceable task-to-generalized-force interface that can serve as the rigid-body backbone for subsequent elastodynamic extensions.

The parameters in Table 4 are constant geometric parameters of the machine. The quantities previously denoted by l_x, l_y, and l_z are the time-varying translational generalized coordinates. No additional workpiece mounting offset is introduced in the numerical model, i.e., ${}^{(c)}\mathbf{p}_{w0} = (x_{w0}, y_{w0}, z_{w0})^T = (0,0,0)^T$ mm. Consequently, with $l_{z4} = 141$ mm, the zero-configuration workpiece-frame origin expressed in the machine-bed frame is $\mathbf{p}_{w0}^{(0)} = (0,0,141)^T$ mm. The corresponding zero-configuration tool-frame origin used in the numerical model is $\mathbf{p}_{t0}^{(0)} = (0,0,376)^T$ mm.

It should be noted that the present validation is intended to assess the consistency of the proposed rigid-body kinematic and dynamic formulation within the nominal machining-motion regime in which the rigid-body assumptions remain applicable. Extremely high-acceleration or high-jerk trajectories may excite structural flexibility, joint/interface compliance, and servo-drive dynamics that are intentionally excluded from the present rigid-body model. Therefore, such operating conditions are not used here as robustness benchmarks for the rigid-body formulation. The present framework is instead designed to provide the unified generalized motion states and wrench interfaces required for subsequent extensions to structural elastodynamics, joint/interface flexibility, and machining-load coupling. Near-singular behavior is treated separately through the analytical singular-value and condition-number analysis of the task-to-screw mapping.

5. Conclusions

The proposed formulation was evaluated through position-level kinematic verification, singularity-conditioning analysis, first- and second-order kinematic checks, and rigid-body force/torque benchmarking. The orientation mapping was shown to have a minimum singular value of $|\sin q_A|$, corresponding to a two-norm condition number of $1/|\sin q_A|$, which quantitatively characterizes the progressive loss of numerical observability as $q_A \to 0$. For the forward–inverse position verification, the position-closure RMSEs ranged from 1.347116×10^{-14} to 3.811000×10^{-14} mm, while the maximum absolute errors ranged from 6.938894×10^{-14} to 1.110223×10^{-13} mm. For the A/C rotary axes, the corresponding RMSEs ranged from 2.019351×10^{-15} to 2.657723×10^{-15} deg, while the maximum absolute errors ranged from 6.361109×10^{-15} to 1.272222×10^{-14} deg. For the rigid-body dynamic validation, the force RMSEs of the X/Y/Z axes ranged from 0.0116695 to 0.0305911 N, with the maximum absolute errors ranging from 0.075609 to 0.531176 N. Whereas the torque RMSEs of the A/C axes ranged from 0.592288 to 1.39897 N mm, the maximum absolute errors ranged from 3.70414 to 8.76912 N mm. These results confirm the numerical consistency of the kinematic mappings and the predictive capability of the rigid-body inverse-dynamics formulation under the investigated trajectory.

The principal contribution of this study is not the introduction of new POE kinematics, Lie-algebraic differentiation, reciprocal-screw theory, Newton–Euler dynamics, or virtual-work theory individually but the construction of a physically consistent analytical architecture connecting the $\mathbb{R}^3 \times S^2$ machining-task representation, admissible rigid-body screw motion, five generalized machine-axis states, and the physical rigid-body chains required for inverse dynamics. In particular, the two-stage task-to-screw-to-joint mapping preserves the physical meaning of the intermediate rigid-body twist and enables the second-order effects associated with task-representation geometry and mechanism-configuration

variation to be explicitly distinguished at the acceleration level. This provides a modular interface between machining-task specification, screw-based kinematics, and generalized rigid-body dynamics.

The present formulation nevertheless remains a rigid-body model. Structural flexibility, joint/interface compliance, servo-drive dynamics, and friction are not explicitly included. Cutting forces and cutting torques are not applied in the present validation; machining loads are retained only through the theoretical external-wrench interface for subsequent extensions. In addition, the high-speed spindle rotation about the tool axis is not introduced as an independent generalized motion, and the associated spindle-rotor inertia and spindle-induced gyroscopic effects are therefore outside the scope of the current model. Exact orientation singularities cannot be resolved from the instantaneous tool-axis direction alone, and the current validation is restricted to the investigated XYZAC architecture and nominal machining-motion regime. Future work will extend the proposed interfaces to elastodynamic, joint-flexibility, servo-dynamic, spindle-rotation, and machining-load coupling models, followed by experimental validation over a wider range of operating conditions.

Author Contributions: Conceptualization, Y.W.; methodology, Y.W.; software, Y.W. and J.K.; validation, Y.W.; formal analysis, Y.W.; investigation, Y.W.; resources, T.W. and Y.W.; data curation, Y.T.; writing—original draft preparation, Y.W.; writing—review and editing, Y.W., J.K. and Y.T.; visualization, Y.W., J.K.; supervision, T.W.; project administration, Y.W. and T.W.; funding acquisition, T.W. All authors have read and agreed to the published version of the manuscript.

Funding: This research was funded by the Thermal Error Compensation Method and Application of Five Axis Machine Tool Based on Intelligent Reconfigurable Numerical Control System grant number 25YFYSHZ00290.

Data Availability Statement: The data presented in this study are available upon request from the corresponding author.

Conflicts of Interest: The authors declare that they have no conflicts of interest.

References

1. Fan, L.; Zhu, Y.; Wu, K.; Zhang, Y.; Gao, L.; Wu, B. A geometry-constraint-driven high-precision cutter contact point determination method for toroidal end mills in five-axis machining of compressor blades. *Aerosp. Sci. Technol.* **2026**, *179* , 113353. [CrossRef]
2. Zhang, K.; Zhang, L.; Yan, Y. Single spherical angle linear interpolation for the control of non-linearity errors in five-axis flank milling. *Int. J. Adv. Manuf. Technol.* **2016**, *87*, 3289–3299. [CrossRef]
3. Wang, X.; Zhang, D.; Li, S.; Guan, Q.; Lu, H.; Zhou, X.; Wang, J.; Sun, Y.; Zuo, D. Actual Tool Pose-Driven Iterative Axis Displacement Compensation for Five-Axis Machine Tools. *Precis. Eng.* **2026**, *102*, 709–726 . [CrossRef]
4. Yang, J.; Altintas, Y. Generalized kinematics of five-axis serial machines with non-singular tool path generation. *Int. J. Mach. Tools Manuf.* **2013**, *75*, 119–132. [CrossRef]
5. Sørby, K. Inverse kinematics of five-axis machines near singular configurations. *Int. J. Mach. Tools Manuf.* **2007**, *47*, 299–306. [CrossRef]
6. Huang, J.; Lu, Y.; Zhu, L.M. Real-time feedrate scheduling for five-axis machining by simultaneously planning linear and angular trajectories. *Int. J. Mach. Tools Manuf.* **2018**, *135*, 78–96. [CrossRef]
7. Huang, K.T.; Gong, H.; Fang, F.; Li, Z. Generation of spherical non-uniform rational basis spline curves and its application in five-axis machining. *Proc. Inst. Mech. Eng. Part B J. Eng. Manuf.* **2015**, *229*, 1104–1117. [CrossRef]
8. My, C.A.; Bohez, E.L. A novel differential kinematics model to compare the kinematic performances of 5-axis CNC machines. *Int. J. Mech. Sci.* **2019**, *163*, 105117. [CrossRef]
9. Lu, Z.; Huo, G.; Li, S.; Liu, X.; Jiang, X. SO(3)-based orientation smoothing for improved rotary-axis motion in five-axis machining. *J. Manuf. Processes* **2026**, *166*, 282–302. [CrossRef]
10. Yaqubi, S.; Barjini, A.H.; Mattila, J. Screw Theoretic Nonlinear PDE Dynamic Model of a Flexible Link Using Body-Fixed Coordinates. *Appl. Math. Model.* **2026**, *158* , 116960. [CrossRef]
11. Müller, A. An overview of formulae for the higher-order kinematics of lower-pair chains with applications in robotics and mechanism theory. *Mech. Mach. Theory* **2019**, *142*, 103594. [CrossRef]
12. Laryushkin, P.; Antonov, A.; Fomin, A.; Essomba, T. Velocity and singularity analysis of a 5-DOF (3T2R) parallel-serial (hybrid) manipulator. *Machines* **2022**, *10*, 276. [CrossRef]

13. Zhang, X.; Yang, M.; Mu, D.; Wang, H. Unified formulas of constrained Jacobian and Hessian matrices for 3T1R overconstrained parallel mechanisms. *Mech. Based Des. Struct. Mach.* **2023**, *51*, 1431–1445. [CrossRef]
14. Wang, Z.; Zhang, W.; Ding, X. Design and analysis of a novel mechanism with a two-DOF remote centre of motion. *Mech. Mach. Theory* **2020**, *153*, 103990. [CrossRef]
15. Selig, J. Applying screw theory to robot dynamics. *J. Appl. Math. Mech.* **1991**, *55*, 159–167. [CrossRef]
16. Gallardo, J.; Rico, J.; Frisoli, A.; Checcacci, D.; Bergamasco, M. Dynamics of parallel manipulators by means of screw theory. *Mech. Mach. Theory* **2003**, *38*, 1113–1131. [CrossRef]
17. Huynh, H.N.; Altintas, Y. Modeling the dynamics of five-axis machine tool using the multibody approach. *J. Manuf. Sci. Eng.* **2021**, *143*, 021012. [CrossRef]
18. Huynh, H.; Altintas, Y. Multibody dynamic modeling of five-axis machine tool vibrations and controller. *Cirp Ann.* **2022**, *71*, 325–328. [CrossRef]
19. Bilgili, D.; Budak, E.; Altintas, Y. Multibody dynamic modeling of five-axis machine tools with improved efficiency. *Mech. Syst. Signal Process.* **2022**, *171*, 108945. [CrossRef]
20. Miao, H.; Wang, C.; Li, C.; Song, W.; Zhang, X.; Xu, M. Nonlinear dynamic modeling and vibration analysis of whole machine tool. *Int. J. Mech. Sci.* **2023**, *245*, 108122. [CrossRef]
21. Akbari, V.O.A.; Mohammadi, Y.; Kuffa, M.; Wegener, K. Identification of in-process machine tool dynamics using forced vibrations in milling process. *Int. J. Mech. Sci.* **2023**, *239*, 107887. [CrossRef]

Disclaimer/Publisher's Note: The statements, opinions and data contained in all publications are solely those of the individual author(s) and contributor(s) and not of MDPI and/or the editor(s). MDPI and/or the editor(s) disclaim responsibility for any injury to people or property resulting from any ideas, methods, instructions or products referred to in the content.